THESIS FOR THE DEGREE OF DOCTOR OF PHILOSOPHY

Heat Transport from On-demand Single-Electron Sources

NASTARAN DASHTI

Department of Microtechnology and Nanoscience (MC2)

Applied Quantum Physics Laboratory

CHALMERS UNIVERSITY OF TECHNOLOGY

Göteborg, Sweden 2019

Heat Transport from On-demand Single-Electron Sources
NASTARAN DASHTI
Göteborg, Sweden 2019
ISBN 978-91-7905-175-4

Doktorsavhandlingar vid Chalmers tekniska högskola
Ny serie Nr 4642
ISSN 0346-718X

ISSN 1652-0769 Technical Report MC2-418
Applied Quantum Physics Laboratory
Department of Microtechnology and Nanoscience (MC2)
Chalmers University of Technology
SE-412 96 Göteborg, Sweden
Telephone: +46 (0)31-772 1000

Cover
Sketch of a coherent conductor fed by a single-electron source.

Printed by Chalmers Reproservice
Göteborg, Sweden 2019

Heat Transport from On-demand Single-Electron Sources
NASTARAN DASHTI
Applied Quantum Physics Laboratory
Department of Microtechnology and Nanoscience (MC2)
Chalmers University of Technology

Abstract

The controlled injection of quantized charge excitations from single-electron emitters into nanoscopic conductors sets the basis for many important applications ranging from metrology to the emerging field of quantum optics with electrons. Successful implementation of these applications relies not only on achieving control on the precision of the particle emission, but also on the energetic properties of the injected particles. These fundamental properties are reflected in transport observables such as time-resolved charge and energy current, as well as the spectral, i.e. energy-resolved current, or the zero-frequency correlators of charge and energy currents, thereby providing a tool for transport spectroscopy.

This thesis deals with two important aspects of the characterization of different time-dependently driven single-electron sources (SES): it provides (i) a detailed analysis of the aforementioned observables and (ii) proposals for the readout of such transport properties. First, we analyze in detail the transport observables in three different SESs. The SESs differ by the characteristics of the applied time-dependent driving voltage and by the degree of particle confinement in the driven conductor; their common feature is that pulses of quantized charge are produced going along with a minimal excitation of the Fermi sea. We point out the impact of the device design and of tunable external parameters, such as temperature, on the transport observables. Second, we theoretically propose ways to experimentally access the transport observables. Charge transport observables are standardly detected for different kinds of sources. In contrast, energy transport– particularly energy-current noise– is more difficult to access experimentally. We propose a setup for the detection of fluctuating charge and energy currents, as well as their correlations, generated by a SES, via reading out frequency-dependent electrochemical-potential and temperature fluctuations in a probe contact. Furthermore, in a second proposal, we investigate how to access the spectral current, giving access to the particles' energy distribution, in an energy-selective detector setup. More specifically, we propose to readout modifications of thermoelectric response coefficients due to the time-dependent driving as a measure of the spectral current. However, importantly, this type of setup also opens completely novel routes: we find that SESs can be used as probes to sense until now unexplored quantum screening effects in thermoelectric transport.

Keywords: single-electron source; charge and heat currents; fluctuations and noise; energy-selective detector, thermoelectric devices.

Acknowledgements

First and foremost, I would like to state my profound appreciation to my supervisor Janine Splettstoesser for her continuous and daily support during my PhD study. I would like to also thank her for giving me the opportunity to do my research in her group. Thank you for all of the constructive criticism which taught me how to find my way. I am also grateful to Peter Samuelsson for all of the useful discussions that we had in Lund, Gothenburg, Skype meetings and most recently, at a Hotel's lobby! Thank you for all the encouragement and motivation that you gave me for the continuation of our common projects.

Many many thanks to Maciej Misiorny. Without him, I would not have made through this work. Thank you for all the supports. I have learned so much from you, both scientifically and also non-scientifically. If all the curves and plots in this thesis and appended papers look nice, it is his legacy. Thanks for the time you spent to solve my stupid problems!

Many thanks to Fatemeh for keeping our long-lasting friendship alive, from Zanjan (a cold and windy city) to Gothenburg (another cold and windy city). It is getting close to a decade that we are together as colleagues and friends. Thank you for your kindness and compassionate heart. Please keep on organizing the weekend activities!

In addition, I thank all my friends and colleagues at Chalmers. Thanks to my past and present office mates; Tobias, Sanakar, Patric and Kevin for your help and all the discussions. Thanks to everyone who contributed to make such a friendly and excellent environment at work; Gio, Jens, Daniel, Joel and the rest of the former and current AQP members. Thanks to Valentina for all the Thursday's lunch and I hope we continue this tradition.

I would like to thank all my Iranian friends who did not let me feel homesick even for a second. Being aboard, far from your family is tough, however, good friends can be your second family who take cares of you. Nima, Mohammad, Fatemeh, Kamran and many more which is impossible to list your names here, thanks for making such a lovely and troublesome family. Merci!

Finally, countless thanks to my family for their ever-existed support and encouragement. Thanks to my mom who has always taught me to fight for my goals in life. Thank you for spending the best years of your life for me, but I regret that I could not be next to you when I was needed. Before I forget to finish this :-), my final thanks go to my husband Saeed; thanks for your continuous supports and cooking delicious foods.

List of publications

This thesis presents an introduction, summary to the following appended papers:

[I] N. Dashti, M. Misiorny, S. Kheradsoud, P. Samuelsson, and J. Splettstoesser, "Minimal excitation single-particle emitters: Comparison of charge-transport and energy-transport properties", Phys. Rev. B **100**, 035405 (2019).

[II] N. Dashti, M. Misiorny, P. Samuelsson, and J. Splettstoesser, "Probing charge- and heat-current noise by frequency-dependent fluctuations in temperature and potential", Phys. Rev. Appl. **10**, 024007 (2018).

[III] S. Kheradsoud, N. Dashti, M. Misiorny, P. P. Potts, J. Splettstoesser, and P. Samuelsson, "Power, Efficiency and Fluctuations in a Quantum Point Contact as Steady-State Thermoelectric Heat Engine", Entropy **21**, 777 (2019).

[IV] N. Dashti, S. Kheradsoud, M. Misiorny, P. Samuelsson, and J. Splettstoesser, " Screening effects in the interplay between thermoelectric response and time-dependent driving", in preparation (2019).

We always refer to these publications as Paper I, II, ..., according to the labeling in the list above.

Contents

1 Introduction

This thesis deals with charge and heat transport and its theoretical aspects in the context of mesoscopic electronic devices, in particular when driven by time-dependent single-electron sources.

The field of mesoscopic physics focuses on *quantum* phenomena in systems whose dimensions fall between the atomic and the macro scale. Specifically, in order to exhibit typical mesoscopic features, at least one of the dimensions of a conductor needs to be smaller than the phase relaxation length (also known as the coherence length). This length is the distance at which an electron wave (in the quantum regime, the electrons act like waves) travels before its initial phase is destroyed. Fulfilling this condition guarantees that the conductor shows non-classical effects. Additionally, on top of the size, the phase relaxation length depends on other factors, e.g., material and temperature. In other words, the mesoscopic physics requires clean samples and low temperatures to become accessible with proper modification of these experimentally controllable factors [1]. Such mesoscopic conductors, which behave both classically and quantum-like as they shrink in size from the macro- to the mesoscale, are the key elements of this dissertation. They play a significant role in the field of nano-electronics which focuses on the analysis of the relevant quantum phenomena that arise due to miniaturization of electronic devices.

A huge advantage of mesoscopic systems is that they are small enough to reveal quantum-mechanical properties, and still sufficiently large to perform electronic transport measurement on them. This fact allows one to perform transport spectroscopy of quantum effects. Quantum interference and entanglement are just two examples of quantum effects that can be addressed, both theoretically and experimentally, by investigating mesoscopic conductors.

Historically, most of the mesoscopic conductors have been implemented in conductors formed in two-dimensional electron gases (2DEG). Such conductors are based on a semiconductor heterostructure made for example from gallium arsenide (GaAs) and aluminum gallium arsenide (AlGaAs) grown on top of that. At the interface of GaAs/AlGaAs, a conducting layer with low density of electrons builds up at very low temperatures (< 1 K) which is referred to as 2DEG [2]. Note that, nowadays many other types of mesoscopic conductors are often used in mesoscopic experiments, such as nanowires, two-dimensional materials and molecular junctions to mention just a few of them. Exploring the feasibility of such device-related application is, however, beyond the scope of this thesis, and we concentrate

here on studying the transport physics in the mesoscopic systems realized in the 2DEGs.

Experiments, which our theoretical work refers to, are mostly don in 2DEGs; however, our predictions are not restricted to those types of the system.

In order to investigate the physics of charge transport, the mesoscopic conductor is typically connected to source and drain ohmic contacts. When applying a voltage between the two contacts (the source and the drain), current flows between them; the properties of this detectable current heavily depend on the quantum properties of the contacted conductor. Such a current consists of many electrons with strong overlap between their wavefunctions, so that it is not possible to distinguish the effect of single electrons. However, for many important applications, having full control over single particles is required. In order to gain such a control, one needs to complement the ohmic contacts with single-electron sources in the mesoscopic conductor. This sets the ground for various practical applications and novel fields of research, ranging from metrology [3] to the emerging field of quantum optics with electrons [4–10] and quantum information processing [11].

In metrological applications [3], one aims to redefine the standard unit of Ampere with an accurate source emitting one discrete electron-charge e per period at GHz frequencies in order to guarantee the measurable current with large enough magnitude. On the other hand, in quantum optics experiments with electrons [9, 12], single-electron sources are often combined with edge states in the quantum Hall regime, which serve as waveguides for electrons. The possibility of achieving a tunable synchronization of electrons emitted from such sources was essential for implementation of fermionic interferometers (such as Mach-Zender interferometer [13] and Hanburry-Brown-Twiss interferometer [4]), in analogy to their photonic counterparts.

The main scope of this thesis is the characterization of such sources.

1.1 On-demand single-electron sources

Indeed, for all of the aforementioned applications, one needs an accurate on-demand single electron source (SES). One of the main examples which is discussed in this thesis is a time-dependently driven mesoscopic capacitor. This has first been realized as a high-frequency SES by Fève and co-workers [4, 14]. Importantly, this source is furthermore realized in the quantum Hall regime to coherently manipulate the emitted particles in fermionic quantum optics. Its working principle is based on Fermi statistics and a quantum confinement which results in the emission of single particles. When a strongly confined system with discrete energy spectrum, a quantum dot (QD), is driven time dependently, the emission of single electrons is expected. The reason is that the energy cost to add or remove one electron from the QD ensures the emission of particles one after the other. In this source, due to the periodically driven QD, single electrons and

holes are pumped to the conductor through a quantum point contact (QPC). The mesoscopic capacitor source is studied extensively in Paper I, and it is then used as an important example in Papers II and IV.

Single electrons can also be emitted without exploiting quantum confinement. Single-electron excitations can be generated by applying a time-periodic bias voltage across the conductor that minimizes additional excitations of electron-hole pairs. In this thesis, we consider an ideal case when a so-called Lorentzian-shaped time-dependent voltage is applied to a coherent conductor [9, 15–17], and as a result only single electrons are generated on top of the Fermi sea without leaving any trace of holes. Another approach is to use the same conductor as in the mesoscopic capacitor setup but fully replace the confinement region by an open conductor element driven by a local time-dependent gate voltage [18]. In this case, the single particles can be emitted by the modulated edge state while the potential landscape of the conductor changes time dependently.

These three sources can emit single particles on top of the Fermi sea as a minimal excitation. Such sources are studied in Paper I where their emission properties are comprehensively compared. There are many other ways to realize SESs [19] which rely on different effects, such as, Coulomb interaction, superconducting gap or the introduced confinement. These effects have been made use of in; (i) superconducting turnstiles [20], by connecting a superconductor island to two normal leads. Single electrons can tunnel from the normal lead to the superconductor if the charging energy and the energy of the gap, are provided by applying a gate or bias voltage; (ii) using surface acoustic waves [6, 7, 21], single electrons from a QD move from one side to the other side of a conductor created by a 2DEG with the velocity of the surface acoustic wave; (iii) in dynamical QDs [5, 22], single electrons are extracted from a 2DEG and trapped in a QD by a time-dependent potential, and then propagated along a channel in the 2DEG, without applying any bias voltage.

Each of these sources mentioned above has advantages for specific types of applications. They can all be imagined as a basis for Paper II and IV, when we propose setups to detect the properties of an arbitrary SES.

1.2 Characterization

In order to exploit the SESs in different applications, the knowledge and understanding of their fundamental properties is essential. Possible methods for the characterization of the SESs is the main focus of this thesis. More specifically, we are interested in accessing fundamental properties of SESs through transport observables used as a *spectroscopy tool*. These observables include the time-resolved charge and energy current, as well as the spectral, i.e., the energy-resolved current, and the zero-frequency correlators of charge and energy currents.

The emitted particles carry charge, hence the first obvious quantity to be stud-

ied is the charge current. In addition, time-dependent properties of the system — which are induced by the driving SES— imply that one has to study the time-resolved charge current rather than only the time-averaged one. The time-resolved charge current reveals when and with which precision particles are emitted. However, since the range of emission time is of the order of nanoseconds [4], the time-resolved charge current is often difficult to access directly in experiments. For this reason, One needs an alternative approach to gain access to the statistics of the emitted particles which, in turn, contains information about the precision of the SES. To do that, one has to resort to the second moment of the statistics, which corresponds to the low-frequency charge-current noise [9, 23–25], and provides information on the number of injected particles, including the neutral electron-hole pair excitations.

Information stored in the transport properties is not limited only to the charge-related properties of the source. In addition to the charge, the emitted particles carry also energy [26–29]. One way to look at the energy distribution of the emitted particles is to study the spectral currents. An alternative tool can be the heat current and the corresponding noise, which contain information about the energetic properties. This fact has in recent years motivated theoretical research on the fluctuations of heat currents, and even mixed correlations of charge and heat currents as a spectroscopic tool for both static [30–35] and driven systems [36–40].

Finally, the question arises in a realistic experiment how to read out the transport properties, which is studied in Paper I in order to characterize the SESs. The detection of the charge-current fluctuations has extensively been studied for different kinds of SESs in Refs. [9, 25, 41, 42]. However, in contrast to the charge currents, the heat currents —both average and fluctuations— are difficult to access experimentally. For instance, Battista and co-workers [38] suggested to measure power fluctuations in order to detect the heat-current noise in the situation when the SES is realized by employing a time-dependent bias voltage. In Paper II, another feasible way to access heat- and charge-current fluctuations caused by SESs is proposed by measuring macroscopic fluctuations of the system [43–45]. To be more precise, we relate the frequency-dependent electrochemical potential and temperature fluctuations in the probe to the bare charge and energy current fluctuations emitted from the SES, which are driven by either gate or bias voltage.

Another challenging quantity to be detected is the spectral current which provides access to the energy distribution of the emitted particles. Despite their difficulty, there are several experimental works on the successful readout of the energy distribution. A highly complex state tomography [46–48] has been developed and performed to address the quantum state of single particles [49]. Furthermore, in Refs. [50, 51], the spectral current for a source that emits single particles far above the Fermi sea, has been measured with the help of an energy-dependent detection barrier. Another way of reading out the energy distribution, particularly in the case of SESs where the Fermi sea is only minimally excited, is given in Paper IV.

In this paper, we propose a setup with an energy-dependent QPC [52–56] to read out the energy distribution of particle current.

The energy-dependent QPC implies that particles can traverse the QPC depending on their energy. Thus, the probability of electrons being transmitted differs from the probability of holes being transmitted, meaning that electron-hole symmetry is broken. With this property that is, the energy-selective barrier, the detection of current gives, in principle, access to the energy distribution of the particles.

However, the energy-selective transmission together with the application of thermal bias is already interesting without SESs, namely it results in thermoelectric effects of the conductor. In Paper IV, we demonstrate, in the presence of SESs that the thermoelectric response coefficients are actually the relevant parameters to directly read out spectral current. To understand this subject, we first study thermoelectric properties of mesoscopic conductors, independent of the SESs characterization. This leads to Paper III, where we investigate the QPC as a steady-state thermoelectric heat engine by studying power, efficiency [57–63], and additionally power fluctuations. The last one, in contrast to macroscopic heat engines, has a significantly large magnitude and impact on the thermoelectric effects. It is worth mentioning that these three quantities are restricted by a so-called Thermodynamic Uncertainty Relation (TUR) [64–66] which has recently been widely studied. We suggest to use such a restriction as a performance quantifier. The trade-off between the large power, high efficiency and small power fluctuations by the TUR is used to analyze the optimization of the performance of the system.

To sum up, the scope of this work is to theoretically study the characterization of the on-demand SESs in the context of transport and thermoelectric quantities. Particularly, we investigate the energetic properties of the SESs by means of heat transport and energy-resolved transport. In general, studying such fundamental properties of the SESs, sets the basis for a controlled and noiseless injection of particles into a coherent mesoscopic conductor, which is in interest of both experimental and theoretical research

1.3 Organization of this thesis

The remaining part of the thesis is divided into six chapters. In the first two chapters we introduce the theoretical method to derive the transport and the thermoelectric quantities in an arbitrary time-dependently driven system, as well as, in a steady state system employed in the thesis and the appended papers. We begin with outlining a scattering approach, particularly, Floquet scattering theory, to study transport quantities in both time-dependently driven and steady state systems. It is followed by Chap. 3 where we study the thermoelectric properties of the systems under consideration.

In Chap. 4, we focus on SESs. We describe three different types of single-electron emitters, as mentioned earlier: a Lorentzian bias voltage, a slowly driven mesoscopic capacitor and a local time-dependent edge-state modulation. In Chap. 5, we present the characterization tools and detection schemes that were used to obtain information on the precision and spectrum of the emitted particles from the introduced sources in previous proposals and experiments. Finally, in Chap. 6, we give a brief overview of the appended papers. The thesis is concluded by summarizing the overall results in Chap. 7.

The thesis includes two appendices that contain detailed auxiliary calculations from the main text. The derivation of the scattering matrix related to the slowly driven mesoscopic capacitor setup is derived as a function of resonant times and energy in Appendix A. In Appendix B, the thermoelectric coefficients in linear-response regime for the transmission function of the QPC being a step function are given.

2 Theoretical description of time-dependent charge and energy transport phenomena in mesoscopic systems

In this chapter, first, we describe a general non-interacting time-dependently driven mesoscopic system that captures essential features of the setups of interest in this thesis. Then, we introduce observables which are experimentally accessible and provide information about the system. Observables, or transport quantities, such as time-resolved charge and energy, as well as spectral currents and zero-frequency correlators of charge and energy currents, are used as spectroscopy tool to characterize the mesoscopic system. Next, we present a scattering matrix approach [67, 68] that is utilized to derive the transport quantities in such a system. In particular, the time-dependent (Floquet) scattering theory [69, 70] is used to describe a time-dependently driven mesoscopic system. Finally, within this framework, we derive explicit expressions for all the transport quantities mentioned above.

2.1 General model

The sketch of a two-terminal setup under consideration is shown in Fig. 2.1. It consists of a coherent conductor (green area) which is connected to left (L) and right (R) contacts. These contacts correspond to electronic reservoirs of effectively non-interacting electrons with well-defined temperature T_α and electrochemical potential μ_α, where $\alpha = \mathrm{L}, \mathrm{R}$. The electronic distribution in each contact is described by the Fermi-Dirac distribution function,

$$f_\alpha(E) = \frac{1}{1 + e^{(E-\mu_\alpha)/k_\mathrm{B}T_\alpha}}. \tag{2.1}$$

In the scatterer area of the conductor, denoted by red-dashed line, there are two key elements : a generic time-dependently driven source, denoted by S (this is the case in Paper I, II and IV, but not in Paper III); and a quantum point contact, denoted by QPC with a possibly energy-dependent transmission (this is

the case in Paper III and IV) [1].

The system is forced out of equilibrium time-dependently by driving either a gate voltage or modulated bias voltage in the region S, see Chap. 4 for a detailed description of distinctive types of setups. However, note that the system can be in a non-equilibrium state also in the absence of the external time-dependent driving which can be achieved by means of a thermal bias or a dc bias voltage, see Chap. 3. As a result of the dc bias or time-dependent driving, particles traverse the conductor ballistically which means that we can in principle learn about properties of the scatterer by studying the flow of these particles.

Since the particles injected into the conductor carry charge and energy, we can study transport quantities such as charge and energy current as well as their corresponding fluctuations and noise. However, when assuming a noiseless time-dependently driven source as the one mentioned in Chap. 4, the latter ones can only be accessed if particles are randomly scattered in the conductor either to the reservoir R or reservoir L. For this purpose, one needs to add e.g. the QP,C which acts as a beam splitter. We can also investigate thermoelectric effects in the system by breaking electron-hole symmetry together with thermal bias, which is the focus of Chap. 3. This becomes possible by employing the QPC as an energy filter which corresponds to the situation when the energy-dependence of transmission probability is relevant.

In the following, we introduce transport quantities as a key tool to characterize the scatterer. Later on, we explain the method, the non-interacting scattering theory, which will be used to derive these observables.

2.2 Definition of transport quantities

Let us introduce the transport quantities, which are the main tools in this thesis to study mesoscopic systems. The derivation of these quantities has been widely studied in my Licentiate Thesis [71], and here, we only introduce them briefly.

Particles that are injected to the conductor carry charges. Therefore, the first quantity to be studied is the charge current. Using the second quantization operators, the charge current operator in the reservoir α is defined by the operators of incoming and outgoing particles from the scatterer and is given by

$$\hat{I}_\alpha(t) = -\frac{e}{h}\iint \mathrm{d}E\,\mathrm{d}E' e^{i(E-E')t/\hbar}\left\{\hat{b}^\dagger_\alpha(E)\hat{b}_\alpha(E') - \hat{a}^\dagger_\alpha(E)\hat{a}_\alpha(E')\right\}. \tag{2.2}$$

In the equation above, $\hat{a}_\alpha(E)$ $[\hat{a}^\dagger_\alpha(E)]$ denotes the annihilation [creation] operator corresponding to an incoming electron from a reservoir α at energy E. Whereas, $\hat{b}_\alpha(E)$ $[\hat{b}^\dagger_\alpha(E)]$ refers to the annihilation [creation] operator corresponding to an outgoing electron to a reservoir α at energy E. Note that throughout this thesis

[1] An energy-independent transmission of the QPC is considered in Paper I and II.

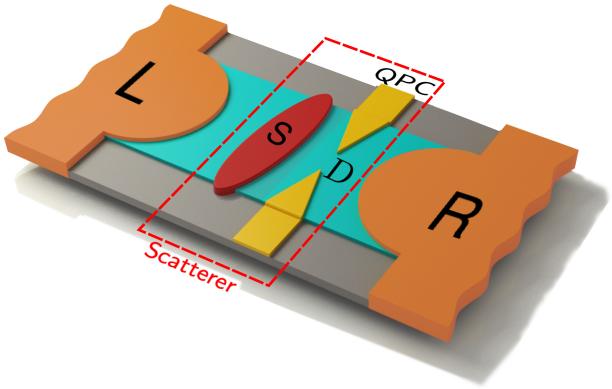

Figure 2.1: *Illustration of a two-terminal mesoscopic system. The coherent conductor (green area) is attached to two electronic reservoirs, left (L) and right (R). The key components of the setup are the time-dependently driven source (S) and an energy-dependent (or independent) quantum point contact (QPC) with transparency D. The QPC is realized by capacitively coupled gates to the conductor (indicated in yellow). The system is brought out of equilibrium either time-dependently with the help of the driven source, S, or in the absence of the source and applying voltage and thermal biases. In both case, particles are injected into the conductor and they are either transmitted through or reflected from the QPC.*

the electron charge is $-e$ while $e > 0$, and the direction of the flowing current is into a reservoir α.

Here, the observable quantities of interest are the time-dependent charge current and the time-averaged charge current. The time-dependent charge current gives information about the type of emitted particles, electrons and holes, in time. This quantity is obtained by evaluating the quantum average of Eq. (2.2), $I_\alpha(t) = \langle \hat{I}_\alpha(t) \rangle$. We assume that the quantum average $\langle \hat{a}^\dagger_\alpha(E)\hat{a}_\alpha(E') \rangle$ is determined by the equilibrium statistical properties of the reservoirs,

$$\langle \hat{a}^\dagger_\alpha(E)\hat{a}_\beta(E') \rangle = \delta_{\alpha\beta}\delta(E - E')f_\alpha(E), \tag{2.3}$$

and $\langle \hat{b}^\dagger_\alpha(E)\hat{b}_\alpha(E') \rangle$ is obtained from the scattering approach introduced in Sec. 2.3 and 2.4. Moreover, the time-averaged charge current is defined as the time integral of the time-dependent charge current over one driving period $\mathcal{T}$,

$$\bar{I}_\alpha = \int_0^{\mathcal{T}} \frac{\mathrm{d}t}{\mathcal{T}} \langle \hat{I}_\alpha(t) \rangle. \tag{2.4}$$

However, by measuring this quantity, one loses some information about the emitted charge which results from the fact that the contributions from electrons (negative charge) and holes (positive charge) cancel each other out due to time averaging of the current.

Independent of their charge, particles carry also energy. Thus, the energy distribution of the emitted particle constitutes another relevant quantity characterizing

features of the system. Specifically, the key quantity to be studied here is the spectral current. The corresponding spectral current operator is obtained from the energy-resolved, time-integrated particle current operator,

$$\hat{i}_\alpha(E) = \int_0^{\mathcal{T}} \frac{\mathrm{d}t}{\mathcal{T}} \int \mathrm{d}E' e^{i(E-E')t/\hbar} \left\{ \hat{b}_\alpha^\dagger(E)\hat{b}_\alpha(E') - \hat{a}_\alpha^\dagger(E)\hat{a}_\alpha(E') \right\}. \tag{2.5}$$

Then, the spectral current is given by the quantum average of this expression, and it can be calculated by employing the scattering approach, see Sec. 2.5. Still, this quantity can hardly be directly accessed in experiments. Another way to acquire information about energetic properties of the particles is to study the energy current. The energy current operator is defined by

$$\hat{I}_\alpha^E(t) = \frac{1}{h} \iint \mathrm{d}E\, \mathrm{d}E' \, \frac{E+E'}{2} \, e^{i(E-E')t/\hbar} \, \left\{ \hat{b}_\alpha^\dagger(E)\hat{b}_\alpha(E') - \hat{a}_\alpha^\dagger(E)\hat{a}_\alpha(E') \right\}. \tag{2.6}$$

Taking the quantum average of the energy-current operator, we obtain the time-dependent energy current.

So far, we have focused on the expectation value of the charge and the energy current. However, these currents can also fluctuate due to the presence of the scatterer. We analyze these fluctuations through their correlator in order to find additional information about the scatterer. Along the same line as Ref. [72], by employing current operators and calculating the quantum statistical expectation value of the correlator between the current fluctuations, we can determine the spectral density of the current noise, $\mathcal{P}_{\alpha\beta}^{XY}(\omega)$,

$$2\pi\delta(\omega+\omega')\mathcal{P}_{\alpha\beta}^{XY}(\omega) = \frac{1}{2}\langle \left\{ \Delta\hat{X}_\alpha(\omega), \Delta\hat{Y}_\beta(\omega') \right\} \rangle, \tag{2.7}$$

where $\Delta\hat{X} = \hat{X} - \langle\hat{X}\rangle$ stands for the fluctuation of the operator $\hat{X}$. Our main focus is on the zero-frequency current noise can be in general derived as follows

$$\mathcal{P}_{\alpha\beta}^{XY}(\omega=0) = \int_0^{\mathcal{T}} \frac{\mathrm{d}t}{\mathcal{T}} \int_{-\infty}^{\infty} \mathrm{d}t' \langle \Delta\hat{X}_\alpha(t)\, \Delta\hat{Y}_\beta(t+t') \rangle. \tag{2.8}$$

The charge-current noise $\mathcal{P}_{\alpha\beta}^{II}$ is then obtained by replacing operators $\hat{X}_\alpha$ and $\hat{Y}_\alpha$ with the charge current operator, $\hat{I}_\alpha$. More importantly, by substituting $\hat{X}_\alpha$ and $\hat{Y}_\alpha$ with $\hat{I}_\alpha^E$, energy-current noise $\mathcal{P}_{\alpha\beta}^{EE}$ is defined. This until today much less studied quantity is of central interest in this thesis, as it allows for obtaining information about energy properties of the time-dependently driven source. The mixed-current noise, which is the consequence of the fact that the emitted particles carry both charge and energy, is given by the correlation between the charge-current operator $\hat{X} = \hat{I}_\alpha$ and the energy-current operator $\hat{Y}_\alpha = \hat{I}^E$. The current noise can be calculated as a correlator of the current fluctuation in different reservoirs, ($\alpha \neq \beta$) or in the same reservoirs ($\alpha = \beta$), where $\alpha, \beta = \mathrm{L}, \mathrm{R}$.

Next, in order to calculate the transport quantities of the mesoscopic system including the scatterer, we need to obtain relatiosn between the outgoing particles and the incoming ones by utilizing the scattering approach. When the system is brought out of the equilibrium by a dc voltage or a thermal bias, rather than an ac voltage, the stationary scattering matrix, Sec. 2.3, is employed. However, in the presence of the time-dependently driven source or ac bias voltage, the system is described by so-called Floquet scattering matrix, Sec. 2.4.

2.3 Energy-dependent stationary scattering matrix

In this section, we consider a simplified scatterer (compared to what is shown in Fig. 2.1), namely when the time-dependent source is not operating, but the QPC transmission is assumed to be energy-dependent. This case is addressed in Paper III and discussed in more detail in Chap. 3. Here, we review only the crucial properties of an energy-dependent stationary scattering matrix [73, 74] which is the framework for studying transport quantities of a system with an energy-dependent QPC.

By applying a voltage or thermal bias between the two reservoirs, particles flow to the conductor and impinge on the QPC. Depending on the shape of the energy-dependent transmission function, particles with a probability amplitude that depends on their energy can be either transmitted or reflected.

Within the stationary scattering approach and second quantization, one can calculate the relation between annihilation [creation] operator of outgoing particles, $\hat{b}_\alpha(E)$ $[\hat{b}^\dagger_\alpha(E)]$, and incoming particles, $\hat{a}_\beta(E)$ $[\hat{a}^\dagger_\beta(E)]$, with

$$\hat{b}_\alpha(E) = \sum_{\beta=\mathrm{L,R}} S_{\alpha\beta}(E)\hat{a}_\beta(E), \tag{2.9}$$

$$\hat{b}^\dagger_\alpha(E) = \sum_{\beta=\mathrm{L,R}} S^*_{\alpha\beta}(E)\hat{a}^\dagger_\beta(E). \tag{2.10}$$

These operators, $\hat{a}_\beta(E)$ and $\hat{b}_\alpha(E)$, are fermionic operators, reflecting the fact that we are dealing with electrons, so that they obey the anti-commutation rules,

$$\begin{aligned} \left\{\hat{a}^\dagger_\alpha(E), \hat{a}_\beta(E')\right\} &= \delta_{\alpha\beta}\delta(E-E'), \\ \left\{\hat{a}^\dagger_\alpha(E), \hat{a}^\dagger_\beta(E')\right\} &= 0, \\ \left\{\hat{a}_\alpha(E), \hat{a}_\beta(E')\right\} &= 0, \end{aligned} \tag{2.11}$$

and analogous relations hold for $\hat{b}_\alpha(E)$.

In the stationary scattering process the energy is conserved and the conservation of particles requires the unitarity of the scattering matrix, i.e.,

$$\sum_\beta S_{\alpha\beta}(E)S^*_{\gamma\beta}(E) = \delta_{\alpha\gamma}. \tag{2.12}$$

As it has been seen in Sec. 2.2, in order to derive currents and their fluctuations, we need to evaluate the quantum statistical average of the products of operators, $\langle \hat{a}^\dagger_\alpha(E)\hat{a}_\beta(E')\rangle$ and $\langle \hat{b}^\dagger_\alpha(E)\hat{b}_\beta(E')\rangle$. Assuming that the reservoirs are at local equilibrium, the statistics of the incoming operators can be determined by Eq. (2.3). The statistics of the outgoing operators, derived using Eq. (2.9) and Eq. (2.10), is thus given by

$$\langle \hat{b}^\dagger_\alpha(E)\hat{b}_\beta(E')\rangle = \sum_{\alpha',\beta'} S_{\alpha\alpha'}(E)S_{\beta\beta'}(E')\langle \hat{a}^\dagger_{\alpha'}(E)\hat{a}_{\beta'}(E')\rangle. \tag{2.13}$$

Note that in the non-equilibrium state, namly large bias voltage and thermal bias, the potential of the conductor can be shifted due to the screening effect that is caused by the accumulation of charge and energy in the conductor. Therefore, the properties of the energy-dependent scattering matrix become dependent on the screening effect, which is further discussed in Chap. 3.

Here, except for Paper III, other appended papers and the main focus of the thesis are about studying on-demand single-electron sources. We even use the QPC with an energy-dependent transmission to characterize the properties of these sources. Thereby, we need to define the framework, within which the time-dependent sources are described.

2.4 Scattering formalism for time-dependent transport

In this thesis, we are interested in the investigation of the generic properties of three distinctive single-electron sources that are based on a time-dependent gate or bias driving of a conductor, see Chap. 4. These sources can be described mathematically with the help of the Floquet scattering matrix. In this section, we explain this method and show how to utilize it to derive transport quantities.

The single-electron source is periodically driven with a frequency $\Omega = 2\pi/\mathcal{T}$, where $\mathcal{T}$ represents the period of the driving. Such a source, together with the QPC, is depicted schematically in Fig. 2.2 as the scatterer (red rectangle), see also the part of the setup in Fig. 2.1 enclosed by the red-dashed line. While being scattered at the time-dependent scatterer, electrons can absorb or emit n energy quanta $\hbar\Omega$ (Floquet quanta), as schematically indicated with the red arrows in Fig. 2.2. According to the Floquet scattering theory [70, 75, 76], a relation between the incoming and outgoing operators can be described by the Floquet scattering matrix. In the following, we present this approach which is described with more detail in my Licentiate Thesis [71] and also in Ref. [77].

Using the Floquet theory, the states that are solutions to the Schrödinger equation for a periodic time-dependent Hamiltonian can be found. Among these states,

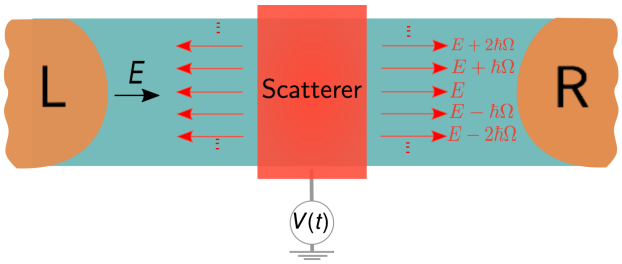

Figure 2.2: *Schematic representation of the system under consideration: A scattering region (red box) is periodically driven with frequency Ω and connected to two electronic reservoirs via leads. Particles with energy E emitted from a reservoir can be reflected or transmitted by the scatterer while absorbing or emitting n Floquet quanta of energy (red arrows).*

we can formally distinguish states impinging onto the scatterer and states outgoing from the scatterer. Here, by using the second quantization representation, these incoming and outgoing states are replaced by relevant annihilation and creation operators. Furthermore, if we assume that the incoming operators are known, the outgoing operators are found from the following relations

$$\hat{b}_\alpha(E_q) = \sum_{\beta=\mathrm{L,R}} \sum_{m=-\infty}^{\infty} S_{\mathrm{F},\alpha\beta}(E_q, E_m)\hat{a}_\beta(E_m), \tag{2.14}$$

$$\hat{b}^\dagger_\alpha(E_q) = \sum_{\beta=\mathrm{L,R}} \sum_{m=-\infty}^{\infty} S^*_{\mathrm{F},\alpha\beta}(E_q, E_m)\hat{a}^\dagger_\beta(E_m). \tag{2.15}$$

Here $S_{\mathrm{F},\alpha\beta}(E_q, E_m)$ denotes the Floquet scattering matrix, where $E_q = E + q\hbar\Omega$. All information about the transport properties of the conductor are encoded in this matrix. Noticeably, the amplitudes of this matrix depend on two energies: the incident energy E_q from a reservoir β, and the scattered energy E_m to a reservoir α. As a result, the number $q - m$ can be understood as the amount of absorbed or emitted energy quanta, which implies that energy is not conserved during the scattering process. However, conservation of the number of particles during the scattering process only after time average leads to unitarity of the Floquet scattering matrix, i.e.,

$$\sum_n \sum_\alpha S^*_{\mathrm{F},\alpha\beta}(E_n, E_m)S_{\mathrm{F},\alpha\gamma}(E_n, E) = \delta_{m0}\delta_{\beta\gamma}. \tag{2.16}$$

As it has been mentioned in the previous section, to derive currents and their fluctuations, one needs to calculate the statistics of the outgoing operators which is given by

$$\langle \hat{b}^\dagger_\alpha(E)\hat{b}_\beta(E')\rangle = \sum_{\alpha',\beta'} \sum_{n,m=-\infty}^{\infty} S^*_{\mathrm{F},\alpha\alpha'}(E, E_n)S_{\mathrm{F},\beta\beta'}(E', E'_m)\langle \hat{a}^\dagger_{\alpha'}(E_n)\hat{a}_{\beta'}(E'_m)\rangle, \tag{2.17}$$

with, $\langle \hat{a}^\dagger_\alpha(E)\hat{a}_\beta(E')\rangle$ given in Eq. (2.3).

So far, we have introduced the Floquet scattering matrix in the energy representation which will be used to describe time-dependently driven sources in Chap. 4. However, it is often also appropriate to introduce the mixed time-energy representation of the scattering matrix which will be proven in Chap. 4, to be particularly convenient for describing the mesoscopic capacitor source. The scattering matrix in the mixed time-energy form can be expressed by means of a partial Fourier transform,

$$S(t,E) = \sum_{n=-\infty}^{\infty} \mathrm{e}^{-in\Omega t}\, S(E_n, E), \tag{2.18}$$

and

$$S(E_n,E) = \int_0^{\mathcal{T}} \frac{\mathrm{d}t}{\mathcal{T}} \mathrm{e}^{in\Omega t}\, S(t,E). \tag{2.19}$$

In such a case, the scattering matrix $S(t,E)$ depends on the energy of the incident particle E and the time t when the particle leaves the scatterer. Inserting the definition of $S(t,E)$, Eq. (2.19), into Eq. (2.16) and making the inverse transformation, the unitarity condition is expressed as follows:

$$\int_0^{\mathcal{T}} \frac{\mathrm{d}t}{\mathcal{T}} \mathrm{e}^{in\Omega t}\, S(t,E_n)\, S(t,E) = \delta_{n0}. \tag{2.20}$$

In this section, we have presented the properties of the Floquet scattering matrix which is employed to describe the time-dependently driven sources. Particularly, one of the key examples of this thesis which is based on a mesoscopic capacitor can be fully described with the mixed energy-time representation $S(t,E)$. However, in the thesis and Papers I, II and IV, the mesoscopic capacitor source is restricted to be driven slowly. In this limit, the scattering matrix is simplified to the stationary scattering matrix with parameters which are dependent on time. This particular type of scattering matrix, so-called frozen scattering matrix, is explained in the next subsection.

2.4.1 Frozen scattering matrix

When the dynamical properties of the scatterer vary slowly as compared to the time which a particle spends in the scatterer, the frozen scattering matrix approximation [70] can be used instead. In such an approximation, a stationary scattering matrix is obtained by freezing the dynamic system at time t, and it is denoted by $S^{(0)}(t,E)$. This matrix which is called the frozen scattering matrix, can characterize the slowly time-dependent scatterer. By Fourier expanding of the scattering matrix, we have:

$$S^{(0)}(t,E) = \sum_{n=-\infty}^{\infty} \mathrm{e}^{-in\Omega t}\, S_n(E). \tag{2.21}$$

Because the Fourier coefficients, $S_n(E)$, of the frozen scattering matrix are determined only by the incident energy E and the transfered energy $n\hbar\Omega$, we can introduce a shorthand notation

$$S(E, E_n) \equiv S_n(E). \tag{2.22}$$

The frozen scattering matrix and its properties are used to describe the slowly time-dependently driven mesoscopic capacitor, as the most important given example in Papers I, II and IV.

So far, we have studied the Floquet scattering matrix for systems which are driven time-dependently by a gate voltage. However, as we mentioned before, the system in the presence of the time-dependent bias voltage can also be described by the Floquet scattering approach which is the purpose of the next subsection.

2.4.2 Scattering amplitude for time-dependent bias voltage

Following the appendix of Ref. [38], In our general model, Fig. 2.1, the time-dependent bias voltages is modulated in the area S and can be treated as time-dependent scattering phases that are picked up when electrons leave or enter the reservoirs in . Then, the reservoirs can still be treated time-independently in the local equilibrium. In other words, by applying a bias voltage $V_{\alpha,\mathrm{b}}(t)$ to the reservoir α, the incoming operator $\hat{a}_\alpha(E)$, which contributes to the current and noise operators, is related to the operators $\hat{a}^0_\alpha(E)$ injected by the reservoir α with equilibrium statistical properties as

$$\hat{a}_\alpha(E) = \sum_{k=-\infty}^{+\infty} c_{\alpha,k}\, \hat{a}^0_\alpha(E_{-k}). \tag{2.23}$$

The quantum average of $\hat{a}^0_\alpha(E)$ obeys the Fermi-Dirac statistics, i.e.,

$$\langle \hat{a}^{0\dagger}_\alpha(E)\hat{a}^0_\beta(E')\rangle = \delta_{\alpha\beta}\delta(E-E')f_\alpha(E), \tag{2.24}$$

while the statistics of the operator $\hat{a}_\alpha(E)$ is modified into

$$\langle \hat{a}^\dagger_\alpha(E)\hat{a}_\beta(E')\rangle = \delta_{\alpha\beta} \sum_{q=-\infty}^{+\infty} \delta(E_q - E')\mathcal{F}_{\alpha,q}(E), \tag{2.25}$$

with the auxiliary function $\mathcal{F}_{\alpha,q}(E)$ is defined as

$$\mathcal{F}_{\alpha q}(E) = \sum_{n=-\infty}^{\infty} c^*_{\alpha,n} c_{\alpha,n+q} f_\alpha(E_{-n}), \tag{2.26}$$

which is the nonequilibrium distribution function due to the time-dependent driving. In the equation above, $c_{\alpha,n}$ is the Floquet scattering amplitude which is defined by

$$c_{\alpha,n} = \int_0^{\mathcal{T}} \frac{dt}{\mathcal{T}} e^{-in\Omega t} c_\alpha(t) \quad \text{with} \quad c_\alpha(t) = e^{i\frac{e}{\hbar}\int_0^t dt' \left(V_{\alpha,\mathrm{b}}(t') - \overline{V}_{\alpha,\mathrm{b}}\right)}. \tag{2.27}$$

Notice that the coefficient $c_\alpha(t)$ depends only on the ac-component of the bias voltage. We use this amplitude to describe the transport quantities in our particular source, that is, the Lorentzian bias voltage studied in detail in Paper I.

2.5 Transport quantities in terms of the scattering matrix

In the following, we present general expressions for transport quantities in terms of the scattering matrix which are used in the rest of the thesis and appended papers to describe the mesoscopic system. These systems are driven time-dependently, by applying either gate or bias voltage. In Appendix B of Paper I, the expressions under consideration are presented in a compact form where both situations, time-dependent driving of the reservoirs, as well as the scatterer, are considered simultaneously. However, here, for simplicity, we discuss these two systems separately.

2.5.1 Time-dependent scatterer

By employing the Floquet scattering matrix, the time-dependent charge current is obtained by evaluating the quantum statistical average of Eq. (2.2), where $\langle \hat{a}^\dagger_\alpha(E)\hat{a}_\alpha(E')\rangle$ and $\langle \hat{b}^\dagger_\alpha(E)\hat{b}_\alpha(E')\rangle$ are given by Eq. (2.3) and Eq. (2.17), respectively:

$$\begin{aligned} I_\alpha(t) &= \langle \hat{I}_\alpha(t)\rangle \\ &= -\frac{e}{h}\sum_\beta \sum_{n,l} \int \mathrm{d}E e^{-il\Omega t} S^*_{\alpha\beta}(E,E_n) S_{\alpha\beta}(E_l,E_n)\{f_\beta(E_n) - f_\alpha(E)\}. \end{aligned} \tag{2.28}$$

Moreover, the time-averaged charge current is given by

$$\bar{I}_\alpha = -\frac{e}{h}\sum_\beta \sum_{m=-\infty}^{\infty} \int \mathrm{d}E \left|S_{\alpha\beta}(E,E_n)\right|^2 \{f_\beta(E_n) - f_\alpha(E)\}. \tag{2.29}$$

In general, these equations show that in order to have a nonzero current, thermal or voltage bias is not required. In other words $\bar{I}_\alpha \neq 0$ even if $f_\alpha(E) = f_\beta(E)$, since we have to consider Fermi function at different energies due to the time-dependent driving.

In analogy to the charge current, using Eq. (2.6), we also obtain the time-dependent energy current

$$\begin{aligned} I^E_\alpha(t) = \frac{1}{h}\sum_\beta \sum_{n,l} \int \mathrm{d}E \left(E + \frac{l\hbar\Omega}{2}\right) e^{-il\Omega t} S^*_{\alpha\beta}(E,E_n) S_{\alpha\beta}(E_l,E_n) \\ \times \{f_\beta(E_n) - f_\alpha(E)\}, \end{aligned} \tag{2.30}$$

and the average energy current is found by integrating the time-dependent energy current over one period $\mathcal{T}$ of the driving:

$$\bar{I}_\alpha^E = \frac{1}{h}\sum_\beta \sum_{n=-\infty}^{\infty} \int \mathrm{d}E\, E\, |S_{\alpha\beta}(E,E_n)|^2 \{f_\beta(E_n) - f_\alpha(E)\}\,. \tag{2.31}$$

Note that in the context of transport measurement, the relevant physical quantity is the heat current. This quantity corresponds to the excess energy carried by particles with respect to the electrochemical potential of the relevant reservoir,

$$J_\alpha(t) = I_\alpha^E(t) + \frac{\mu_\alpha}{e} I_\alpha(t). \tag{2.32}$$

Here, we have assumed $V_{\alpha,\mathrm{b}}(t) = 0$. The time-averaged heat current is then derived by taking the average of the energy and the charge current.

The zero-frequency noise is obtained by

$$\begin{aligned}\mathcal{P}_{\alpha\beta}^{XY} =& \frac{1}{h}\sum_{\gamma,\eta}\sum_{n,m,q}\int \mathrm{d}E\, x y_q\, f_\gamma(E_n)\, [1 - f_\eta(E_m)] \\ &\times S^*_{\alpha\gamma}(E,E_n) S_{\beta\gamma}(E_q,E_n) S_{\alpha\eta}(E,E_m) S^*_{\beta\eta}(E_q,E_m) \\ &- \frac{1}{h}\sum_q \int \mathrm{d}E\, x y_q\, |S_{\alpha\beta}(E,E_q)|^2 f_\beta(E_q)\, [1 - f_\beta(E_q)] \\ &- \frac{1}{h}\sum_q \int \mathrm{d}E\, x_q y\, \left[|S_{\beta\alpha}(E,E_q)|^2 - \delta_{\alpha\beta}\delta_{q,0}\right] f_\alpha(E_q)\, [1 - f_\alpha(E_q)]\,. \end{aligned} \tag{2.33}$$

The expression for the charge-current noise, $\mathcal{P}^{II}$, is obtained when $x = y = -e$ and $x_q = y_q = -e$. On the other hand, the energy-current noise, $\mathcal{P}^{EE}$, is acquired by replacing $x, y = E$ and $x_q = y_q = E + q\hbar\Omega$. Finally, the mixed-current noise, $\mathcal{P}^{IE}$, is given when $x = E$ and $x_q = E + q\hbar\Omega$ and $y_q = y = -e$ or the other way around.

We have formulated the transport quantities, using the Floquet scattering matrix in the presence of the time-dependent potential energy. However, for the stationary case, Sec. 2.3, the transport quantities are simply obtained by substituting $S_{\alpha\beta}(E,E_n)$ with $S_{\alpha\beta}(E)\delta_{n0}$ in the above equations.

2.5.2 Time-dependent bias voltage

Along the same line as in the previous subsection, by using Eq. (2.23), we describe the transport quantities in the presence of a time-dependent bias voltage. To calculate these quantities one needs to evaluate the quantum average, $\langle \hat{a}_\alpha^\dagger(E)\hat{a}_\alpha(E')\rangle$ which is given by Eq. (2.25).

The time-dependent charge and energy currents are obtained now in the form

$$I_\alpha(t) = -\frac{e}{h}\sum_\beta\sum_q \int \mathrm{d}E e^{-iq\Omega t} |S_{\alpha\beta}(E)|^2 \{\mathcal{F}_{\beta q}(E) - \mathcal{F}_{\alpha q}(E)\}, \tag{2.34}$$

and

$$I_\alpha^E(t) = \frac{1}{h}\sum_\beta\sum_q \int \mathrm{d}E \left(E + \frac{q\hbar\Omega}{2}\right) e^{-iq\Omega t}|S_{\alpha\beta}(E)|^2\{\mathcal{F}_{\beta q}(E) - \mathcal{F}_{\alpha q}(E)\}, \quad (2.35)$$

where the nonequilibrium distribution due to time-dependent driving, $\mathcal{F}_{\alpha,q}(E)$, is given by Eq. (2.26). By considering this model the heat current for $V_\mathrm{b}(t) \neq 0$ can be obtained by Eq. (2.32). Next, the current noise is given by

$$\begin{aligned}\mathcal{P}_{\alpha\beta}^{XY} = \frac{1}{h}\int dE \sum_{l=-\infty}^{\infty} xy_l \Big\{ &\delta_{\alpha\beta}\,\mathcal{F}_{\alpha,l}(E)\big[\delta_{l0} - \mathcal{F}_{\alpha,-l}(E_l)\big] - |S_{\alpha\beta}(E)|^2 \\ &\times \mathcal{F}_{\beta,l}(E)\big[\delta_{0l} - \mathcal{F}_{\beta,-l}(E_l)\big] - |S_{\beta\alpha}(E)|^2\,\mathcal{F}_{\alpha,l}(E)\big[\delta_{l0} - \mathcal{F}_{\alpha,-l}(E_l)\big] \\ &+ \sum_{\gamma\lambda}\sum_{m=-\infty}^{\infty} S^*_{\alpha\gamma}(E)S_{\alpha\lambda}(E)S^*_{\beta\lambda}(E)S_{\beta\gamma}(E)\,\mathcal{F}_{\gamma,l}(E)\big[\delta_{m0} - \mathcal{F}_{\lambda,m}(E_{-m})\big]\Big\}.\end{aligned} \quad (2.36)$$

As mentioned in the previous subsection, by replacing x, y by e and/or E, charge-, energy- and mixed current noise can be acquired. This formalism is used when we study Lorentzian-shaped bias voltage in Paper I.

In this chapter, we formulated the transport quantities in the two-terminal setup with the central scatterer by employing the scattering theory. The different kinds of scatterers is considered. They include, first, the energy-dependent scatterer, which is described by the stationary scattering matrix, and second, the time-dependently driven scatterer by either a gate voltage or a bias voltage which is presented by the Floquet scattering matrix. This theoretical approach fully covers our study in this thesis and the appended papers. Furthermore, in Chap. 3, we present the possible thermoelectric coefficients of the system in the framework of scattering theory. The transport, together with thermoelectric quantities, will be used as a tool to characterize the key element of the introduced setup, i.e., single-electron sources, in Chap. 4 which is also studied in Paper IV.

3 Thermoelectric effect at the nanoscale

In this chapter, we focus on analyzing thermoelectric features of mesoscopic conductors. The example system we focus on, is a setup involving a quantum point contact (QPC) with energy-dependent transparency [52, 53, 57, 58]. We start this chapter by presenting an overview on using a QPC as an energy-selective barrier, and then, as a thermoelectric device which operates under an applied thermal bias. Further, we introduce the specific setup of interest with an energy-dependent QPC. We describe the QPC potential and how it leads to a transmission probability with step-like dependency on energy. Thereafter, we explain the screening effects that are observed when an applied bias across the sample leading to charge pile-up at the QPC, modifies the local potential landscape. We analyze the thermoelectric transport coefficients in the-linear response regime while the system is either in a stationary state (see Paper III), or in the presence of an arbitrary time-dependently single-electron sources (SES), of which we introduce several in Chap. 4. In the latter case, the screening effects become noticeable and modify the thermoelectric response coefficients. This setup allows for two different aspects of spectroscopy (see Paper IV); first, modified thermoelectric quantities are used as a tool to characterize the SES. Second, the screening effects is sensed by using the SES as a probe.

3.1 QPC as thermoelectric device

By considering QPC with an energy-dependent transmission probability, one can filter the transport of particles based on their energy, which results in breaking the symmetry between the probability of transmitted electrons and holes. This energy-selective QPC, when applying thermal bias, allows for the realization of thermoelectric effects in the conductor.

Indeed, the QPC in the mesoscopic conductors has been the device to realize thermoelectric effects [53, 78]. Since then, many studies on the thermoelectric properties of QPCs have been done [52, 54, 55, 79, 80]. It has also been used as a miniature thermometer [53], by taking advantage of the fact that the conductance broadening is proportional to the temperature. In these works, the considered energy filtering is a step-like function [52, 53, 80] which is a consequence of the saddle-point electrostatic potential of the QPC, explained in Sec. 3.2. Other kinds

of filtering have also been employed by replacing the QPC with e.g., a QD, which creates Lorentzian or Dirac delta functions in the transmission [56, 79, 81].

Despite those early studying, analyzing the QPC as a thermoelectric device is still an ongoing research topic. In heat engines or refrigerators, the optimal performance of a device is of crucial importance. In the case of a heat engine, the electrical power product, P, and the efficiency, $\eta = P/J$, where J is the heat current flow into the device, here the QPC, are well-known quantifiers that are used to optimize the performance of the system. An extensive investigation has been done on the optimal performance of thermodynamic devices, especially the efficiency at the maximum power which in the linear response regime is limited by the Curzon-Ahlborn efficiency [61–63, 80–85].

Besides the maximized efficiency and the power, considering minimized fluctuations is also a way to optimize the performance of the system. This comes from the fact that the fluctuations in small devices, in contrast to the macroscopic systems, has a relevantly large magnitude. Therefore, studying combination of efficiency, power and fluctuations become of interest in this context. To do that, the recent study on Thermodynamic Uncertainty Relations(TUR) [64, 65] suggests us to define a combined performance quantifier which is restricted by the TUR bound. This is the subject of Paper III.

In Paper IV, thermoelectric effects of the QPC is used in the context of the SESs characterization. In this paper, we use of thermoelectric response coefficients to directly read out spectral current which gives information about energy distribution of the emitted particle.

3.2 QPC Setup

In Fig. 3.1, we schematically show a system which is brought out of equilibrium by applying electrochemical potential and temperature differences between the two reservoirs. We assume that the reservoir R is the hot one while the reservoir L is the cold one and take the temperature of the reservoir L as the reference (background) temperature, meaning that $T_{\mathrm{L}} = T_0$ and $T_{\mathrm{R}} = T_0 + \Delta T$ while $\Delta T > 0$. On the other hand, the electrochemical potentials are defined as $\mu_{\mathrm{L}} = \mu_0$ and $\mu_{\mathrm{R}} = \mu_0 + \Delta\mu$. Here, μ_0 represents the electrochemical potential in the absence of a bias voltage. We use $\mu_0 = 0$ as the reference energy. Two reservoirs are connected to each other via a QPC with transparency $D(E)$. Particles from the reservoirs flow into the conductor and they are reflected or transmitted at the QPC depending on their energy. In the following, we elaborate on the QPC which acts as an energy filter in the setup.

In general, a QPC is used to constrict the flow of electrons in different types of nanoscale conductors such as a two-dimensional electron gas (2DEG). Two metallic gates with a distance of the order of hundreds of nms between them, are connected capacitively to the top of the conductor through a layer of insulator

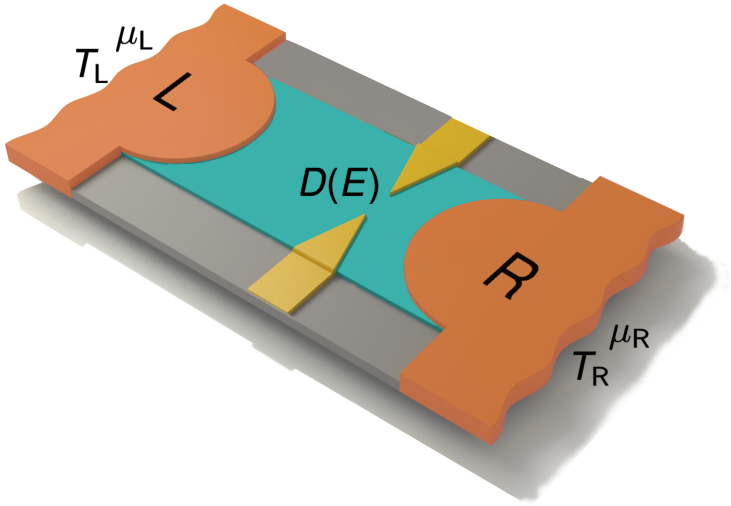

Figure 3.1: *Illustration of the two-terminal system with a central quantum point contact (QPC). The emitted electrons from reservoirs left (L) and right (R) are scattered at the QPC which is characterized by the energy-dependent transparency $D(E)$. The reservoir L is kept at electrochemical potential $\mu_L = \mu_0$ and temperature $T_L = T_0$ (cold reservoir). The reservoir R is characterized by electrochemical potential $\mu_R = \mu_0 + \Delta\mu$ and temperature $T_R = T_0 + \Delta T$ (hot reservoir).*

material [86, 87], see a yellow area in Fig. 3.1. The QPC is defined by applying a negative voltage to the gate such that a short and narrow constriction for the flow of particles is created in between the two gates. However, also in nanowires, similar constrictions can be realized which can be either achieved by means of interfaces or controlled by finger gates [81].

As we mentioned above, the QPC can be established in a 2DEG in the form of an electrostatic constriction induced with a pair of split gates. Electrons can be transmitted or reflected at the potential, created by the split gates in the narrow bottleneck. The potential is approximated as a saddle point shape, near the narrowest point of the QPC. This approximation is achieved by considering the lowest order of the expanded potential around the appropriate positions x and y, which is given by [52, 88]

$$U(x,y) = U_0 - \frac{1}{2}m\omega_x^2 x^2 + \frac{1}{2}m\omega_y^2 y^2. \tag{3.1}$$

Above, x and y denote longitudinal and transverse directions, respectively. The curvature of the saddle is defined by ω_x and ω_y, while U_0 is the potential at the saddle. The total energy of incident particles is obtained by adding the kinetic energy, $p^2/(2m)$. The eigenstates of the resulting Hamiltonian can be separated into a transverse component with the energy $E_n = \hbar\omega_y(n+1/2)$, and a longitudinal component with an effective potential $U_0 + \hbar\omega_y(n+1/2) - 1/2\omega_x^2 x^2$. This effective potential is regarded as the band bottom of a quantum channel around the saddle point. Particles can be transmitted through the QPC, if their energy is larger

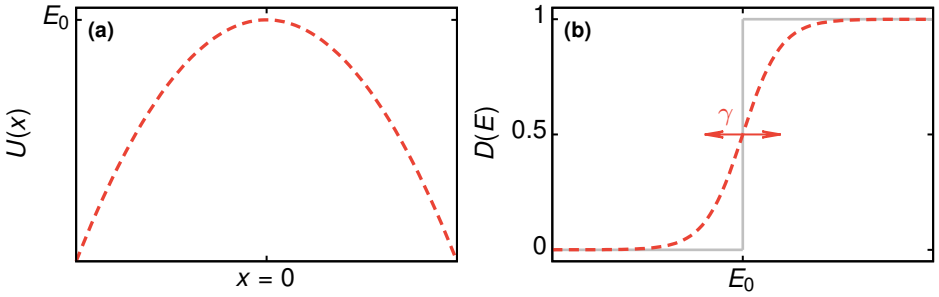

Figure 3.2: *(a) The electrostatic potential of QPC, Eq. (3.3), shown in terms of the longitudinal direction, x. (b)The transmission probability, Eq. (3.4), shown as a function of energy, with a step positioned at energy E_0 and smoothness γ. The gray line shows the step function when $\gamma \to 0$.*

than the threshold energy,

$$E_n = U_0 + \hbar\omega_y(n + \frac{1}{2}), \tag{3.2}$$

with n referring to the number of channels. In the present discussion we consider only one channel, meaning that $n = 0$. Hence, the QPC is effectively one dimensional along the x-axis, and its electrostatic potential is reduced to

$$U(x) = E_0 - \frac{1}{2}m\omega_x^2 x^2, \tag{3.3}$$

where $E_0 = U_0 + \hbar\omega_y/2$ denotes the top of the potential and $m\omega_x^2$ represents the width of the potential which is shown in Fig. 3.2(a). Then, as a consequence, the transmission function from Ref. [89] can be calculated as

$$D(E) = \frac{1}{1 + \exp\left(\frac{-E+E_0}{\gamma}\right)}. \tag{3.4}$$

Here, E_0 stands for the position in energy of the step-like function and $\gamma = \hbar\omega_x/(2\pi)$ is the smoothness. This transmission probability is shown in Fig. 3.2(b). In experimental papers [53, 86, 87], where the conductor is realized in a 2DEG, a smoothness γ of the order of 1 meV or smaller than 1 meV is estimated. However, in Ref. [81], for a different type of a conductor, that is, a quantum wire, γ is expected to be in the order of 1 μeV. Note that, when the smoothness is smaller than other relevant energy scales, we can set $\gamma \to 0$, and the transmission function approaches a step function, i.e., $D(E) = \Theta(E - E_0)$.

So far, we have described the properties of a QPC in an equilibrium situation. However, in general, the transmission probability of the QPC depends on the potential landscape of the conductor. When applying voltage and temperature differences, charges are accumulated in the scattering area, and hence, due to

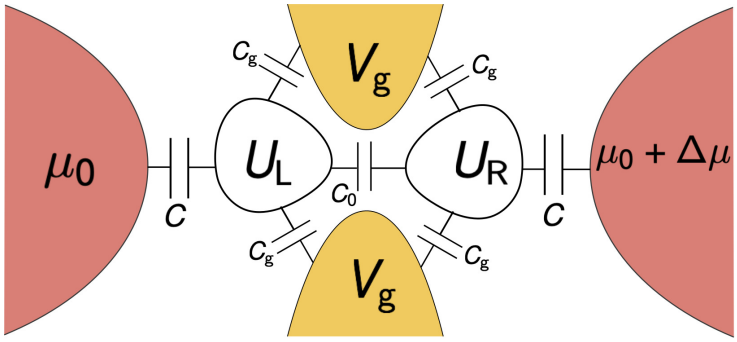

Figure 3.3: *Schematic top-view of a QPC, showing regions L and R where the charge is not screened. These regions are connected to two reservoirs with capacitance C and to the gate with capacitance C_g.*

screening effects, the QPC potential is modified. In the next section, we study how screening affects the QPC properties and the transport quantities of the system. Therefore, it is more convenient to use the notation $D(E, U_{\mathrm{QPC}})$ for the transmission function of the QPC, where U_{QPC} is the potential landscape resulting from screening effects.

3.3 Screening effects and gauge invariance

When the system is forced out of equilibrium, due to applied temperature and voltage differences, the charge can be accumulated around the QPC which leads to screening effects. The screening properties in a metallic conductor can usually be neglected, whereas in semiconductors it has long range effects. This effect [90–92] causes the potential landscape to shift. More explicitly, potential regions U_{L} and U_{R} are built up, see Fig. 3.3, the QPC potential is then defined by $U_{\mathrm{QPC}} = U_{\mathrm{L}} + U_{\mathrm{R}}$ which depends on voltages and temperature. In equilibrium, or when the screening effects are negligible, U^0_{QPC} is considered to be constant and it is absorbed into the scattering properties of the QPC. The transmission function is then denoted by $D(E, U^0_{\mathrm{QPC}}) \equiv D(E)$.

Due to the potential shift, the scattering matrix of the QPC, in the screening length, gets an energy-dependent phase [60, 93], and can be written as

$$S(E) = e^{i\phi(E,U_{\mathrm{QPC}})} \begin{pmatrix} i\sqrt{1 - D(E, U_{\mathrm{QPC}})} & \sqrt{D(E, U_{\mathrm{QPC}})} \\ \sqrt{D(E, U_{\mathrm{QPC}})} & -i\sqrt{1 - D(E, U_{\mathrm{QPC}})} \end{pmatrix}. \tag{3.5}$$

Here $\phi(E, U_{\mathrm{QPC}})$ depends on screening properties through the screening length.

Furthermore, in order to derive the transmission probability, $D(E, U_{\mathrm{QPC}})$, we need to define the QPC potential U_{QPC}. In our setup as it is shown in Fig. 3.3, the potential regions U_{L} and U_{R} are capacitively connected to the reservoirs with

capacitance C and to the gate with capacitance $C_{\rm g}$. The coupling between two potential regions, with capacitance C_0, does not affect the result of our setup. The general model, considering further capacitances, is discussed in the appendix of Paper IV. The voltage and temperature dependency of the QPC potential is described through geometric (classical) capacitances but also by quantum properties of accumulated charges. This has been nicely shown in the weakly non-linear regime, where the potential, $U_{\rm QPC}$, can be expanded up to the first order [60]

$$U = U_{\rm eq} - \xi\frac{\Delta\mu}{e} + \chi\Delta T. \tag{3.6}$$

where ξ and χ are characteristic potentials that describe the internal changes of the system due to the shift of voltage and temperature. These coefficients are derived by investigating charge conservation in the system discussed in Paper IV and are defined as

$$\xi = \frac{2C+d}{2C+d+2C_{\rm g}},\quad \chi = \frac{d^E}{2C+d+2C_{\rm g}}. \tag{3.7}$$

Here, the charge and entropy injectivities

$$\begin{aligned} d &= -e^2\int dE\nu(E)\frac{df_0(E)}{dE}\\ d^E &= -e^2\int dE\frac{E}{k_{\rm B}T_0}\nu(E)\frac{df_0(E)}{dE}, \end{aligned} \tag{3.8}$$

contain information on carriers of charges and entropy, E/T_0, respectively, which enter to the two potential regions. The total density of state, ν_α^e is given by

$$\nu(E) = \frac{1}{2\pi i}{\rm tr}\Big[\hat{S}^\dagger\frac{d\hat{S}_{\beta\alpha}}{dE}\Big] = \frac{1}{2\pi i}\frac{d\phi(E)}{dE}. \tag{3.9}$$

This shows that if the phase in the scattering matrix, Eq. (3.5), is energy independent, the density of state vanishes, $\nu(E) = 0$, and as a consequence there is no charge and entropy injectivities and therefore no quantum screening effects.

Considering screening effects guarantees that electric transport under a global potential shift is Gauge invariant. Note that in the non-linear transport regime, Gauge invariance in general is not fulfilled in scattering theory when screening effects are neglected [90, 91, 94, 95].

In Paper III, we consider a simpler model where it is assumed that the scattering matrix, Eq. (3.5), has an energy-independent phase which leads to zero charge and entropy injectivities. However, we still have the voltage dependency of the potential through the geometric capacitances. Nevertheless, by applying a symmetric bias voltage this dependency is canceled out. The gate voltage dependency of the QPC potential is absorbed into the step energy, i.e.,

$$E_0(V_{\rm g}) = E_0 + eC_{\rm g}V_{\rm g}/(2C+C_{\rm g}) \equiv E_0. \tag{3.10}$$

Moreover, since the entropy injectivity is zero, the temperature dependency of the QPC potential in this setup does also not enter. Note that in many previous studies the potential shift due to screening effects has not been considered in the transport quantities for different reasons such as symmetric design and linear properties of the setup [80–85, 95]. However, these assumption guarantee that the transport quantities are invariant under a global potential shift.

In the following sections, we analyze two different regimes. First, we describe the transport quantities in the linear response regime of the steady-state system. Hence, screening effects are negligibly small and we can develop a simple and intuitive picture of the thermoelectric properties. Second, in order to sense the screening effects, one of our main findings is that it is convenient to study ac-transport quantities induced by an additional SES in the linear response regime of voltage and temperature differences. From a different perspective, the impact of screening effects on the thermoelectric properties allows us to characterize the SESs. Both of the mentioned topics in the latter regime are the subject of Paper IV.

3.3.1 Linear response regime

In mesoscopic samples, along the same line as in macroscopic systems, we can analyze the well-known thermoelectric effects. For instance, a thermal bias can induce a bias voltage due to energy-dependent transmission of the QPC which is called the Seebeck effect. Or a bias voltage can induce a thermal bias which is referred to as the Peltier effect. This can be shown in the linear response regime where the variation of the voltage and temperature differences around the equilibrium are small. In this regime, the charge and heat currents depend linearly on the voltage and temperature differences via the so-called Onsager matrix [55],

$$\begin{pmatrix} I_{\mathrm{R}} \\ J_{\mathrm{R}} \end{pmatrix} = \begin{pmatrix} G & L \\ M & K \end{pmatrix} \begin{pmatrix} \Delta\mu/e \\ \Delta T \end{pmatrix}. \tag{3.11}$$

Here, charge and energy conservation results in $I_{\mathrm{R}} = -I_{\mathrm{L}}$ and $J_{\mathrm{R}} = -J_{\mathrm{L}}$. Only in non-linear response, Joule heating leads to a breakdown of heat current conservation.

The thermoelectric coefficients, G, L, K and M, which we refer to as "standard" TE-coefficients, are given by

$$G = \frac{e^2}{h} \int dE\, D(E) \left(-\frac{\partial f_0(E)}{\partial E} \right), \tag{3.12}$$

$$L = -\frac{M}{T_0} = \frac{e}{h} \int dE\, D(E)\, \frac{E}{T_0} \left(-\frac{\partial f_0(E)}{\partial E} \right), \tag{3.13}$$

$$M = -\frac{e}{h} \int dE\, D(E)\, E \left(-\frac{\partial f_0(E)}{\partial E} \right), \tag{3.14}$$

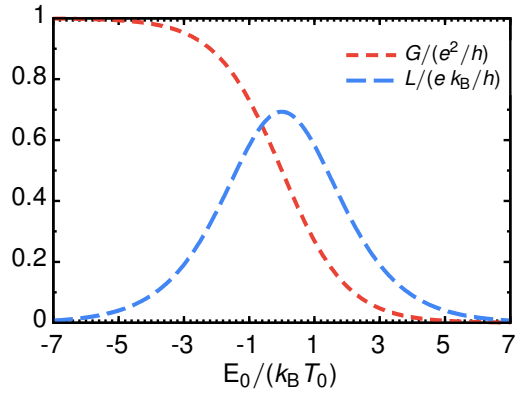

Figure 3.4: *Electrical conductance, G, and the thermoelectric coefficient, L, for a transmission probability of the QPC approximated by a step function, $D(E) = \Theta(E - E_0)$.*

$$K = -\frac{1}{h}\int dE\, D(E)\, \frac{E^2}{T_0}\left(-\frac{\partial f_0(E)}{\partial E}\right). \tag{3.15}$$

Here, $f_0(E)$ refers to the Fermi function at equilibrium namely in the absence of voltage and temperature biases,

$$f_0(E) = \frac{1}{1+\exp[E/(k_B T_0)]}. \tag{3.16}$$

Note that G and K represent the electrical and thermal conductance, whereas L and M are called the thermoelectric coefficients, respectively. Fig. 3.4 shows the behavior of L and G when the transmission probability of the QPC is given by a step function, $D(E) = \Theta(E - E_0)$, for more details of the calculation see Appendix B. As it is shown in Fig. 3.4, when $E_0 \to -\infty$, meaning that the transparency acts energy-independently, the thermoelectric coefficients L and also $M = T_0 L$ become zero. In other words, when the electron-hole symmetry is preserved in the system, no thermoelectric effect takes place.

In the linear response regime, as we have discussed, the screening effects is not noticeable. According to Refs. [90–92], this effect starts playing a role in a weakly non-linear response regime or as we show in Paper IV, when an additional time dependent driving is applied in the ac-transport regime. For this reason, we move on to the linear response regime with an additional time-dependent driving and study the resulting thermoelectric effects.

3.3.2 Interplay between SES and linear response regime

Adding a time-dependently driven SES as introduced later in Chap. 4 in the linear response regime leads to noticeable screening effects in the currents.

We write the currents of the time-dependent system in this regime as

$$\begin{pmatrix} I_{\mathrm{R}} \\ J_{\mathrm{R}} \end{pmatrix} = \begin{pmatrix} G + G_{\mathrm{s}} & L + L_{\mathrm{s}} \\ M + M_{\mathrm{s}} & K + K_{\mathrm{s}} \end{pmatrix} \begin{pmatrix} \Delta\mu/e \\ \Delta T \end{pmatrix} + \begin{pmatrix} I_{\mathrm{dir}} \\ I^{E}_{\mathrm{dir}} \end{pmatrix}. \tag{3.17}$$

Here $I_{\mathrm{s}}^{\mathrm{dir}}$ and $J_{\mathrm{s}}^{\mathrm{dir}}$ correspond to the 'direct' current from the SES, modified by the energy-dependent transmission,

$$I_{\mathrm{s}}^{\mathrm{dir}} = \frac{e}{h} \sum_n |S_n|^2 \int dE\, D(E)\, \left[f_0(E) - f_0(E_n)\right], \tag{3.18}$$

$$I_{\mathrm{s}}^{E,\mathrm{dir}} = \frac{-1}{h} \sum_n |S_n|^2 \int dE\, D(E)\, E \left[f_0(E) - f_0(E_n)\right]. \tag{3.19}$$

Furthermore, G_{s} and M_{s} are the corrections of the electrical conductance and thermoelectric coefficient, respectively, due to the response of the SES current caused by the screening effects due to electrochemical potential differences. They are given by

$$G_{\mathrm{s}} = \xi \frac{e^2}{h} \sum_n |S_n|^2 \int dE\, D(E) \left[\frac{\partial f_0(E)}{\partial E} - \frac{\partial f_0(E_n)}{\partial E}\right], \tag{3.20}$$

$$M_{\mathrm{s}} = -\xi \frac{e}{h} \sum_n |S_n|^2 \int dE\, D(E)\, \frac{\partial}{\partial E} \left\{E \left[f_0(E) - f_0(E_n)\right]\right\}. \tag{3.21}$$

Finally, L_{s} and K_{s} represent the corrections to the thermal conductance and thermoelectric coefficient, respectively, due to the response of the SES current caused by the screening effects due to temperature differences, and they have the following form

$$L_{\mathrm{s}} = \chi \frac{k_{\mathrm{B}} e}{h} \sum_n |S_n|^2 \int dE\, D(E) \left[\frac{\partial f_0(E)}{\partial E} - \frac{\partial f_0(E_n)}{\partial E}\right], \tag{3.22}$$

$$K_{\mathrm{s}} = -\chi \frac{k_{\mathrm{B}}}{h} \sum_n |S_n|^2 \int dE\, D(E)\, \frac{\partial}{\partial E} \left\{E \left[f_0(E) - f_0(E_n)\right]\right\}. \tag{3.23}$$

These correction to the TE-coefficients are the result of a combination of the time dependency and the screening effect discussed above.

We identify two highly important consequence from this finding. In Paper IV, first, we suggest to study the properties of the QPC due to the screening effect by using the well-established SES as a probe. Second, we propose to characterize the properties of SESs by studying the modified thermoelectric coefficient of the QPC.

4 On-demand single-electron sources

Previously in Chap. 2, we have introduced the general model of the setup that we study in this thesis and the theoretical framework to describe it. In this chapter, we elaborate further on the single-electron source (SES), which is the most important element of this thesis. There are many different approaches to achieve the emission of single particles [19]. We are specifically interested in the emission of single-particle pulses from three distinctive types of sources. Their common feature is that they only minimally excite the Fermi sea. However, they differ by their driving protocol and by the degree of particle confinement in the driven conductor. First, in Sec. 4.1, we describe a SES that emits single particles with a particular shape of the bias voltage, which is known as the time-dependent Lorentzian bias [9, 15–17]. Then, in Sec. 4.2, we consider a SES involving the quantum-confinement regime where single particles are generated with a time-dependently driven mesoscopic capacitor [4]. Finally, in Sec. 4.3, we discuss a SES where a local gate-voltage modulation of a quantum Hall edge state which allows for emission of single particles by locally driving without confinement [18]. These sources serve as particle input to the setup that is introduced in Chap. 2, namely a conductor with a possibly QPC with an energy-dependent transparency $D(E)$. We describe these different types of single-electron emission processes by employing the Floquet scattering matrix, which has been used in the Papers I, II, IV.

4.1 Lorentzian bias voltage

It is a known fact that by applying a regular periodic bias voltage across a conductor, for instance of a sinusoidal shape on a conductor, possibly a large number of electron-hole pairs is excited. However, Levitov and co-workers [15–17] have predicted that a Lorentzian-shaped, time-dependent potential fulfilling the condition $eV = \hbar\Omega$ can generate single-electron excitations on top of the surface of the Fermi sea, without the trace of additional electron-hole pairs.

The experimental existence of such electron-like particles has recently been confirmed by noise measurements [9, 25]. The setup which is used in the experiment and also in this thesis, is shown in Fig. 4.1. In the experiment of Ref. [9], two ohmic contacts, reservoirs L and R, are connected to a ballistic conductor which is a 2DEG made of GaAs/GaAlAs. On top of this heterojunction, a QPC is formed

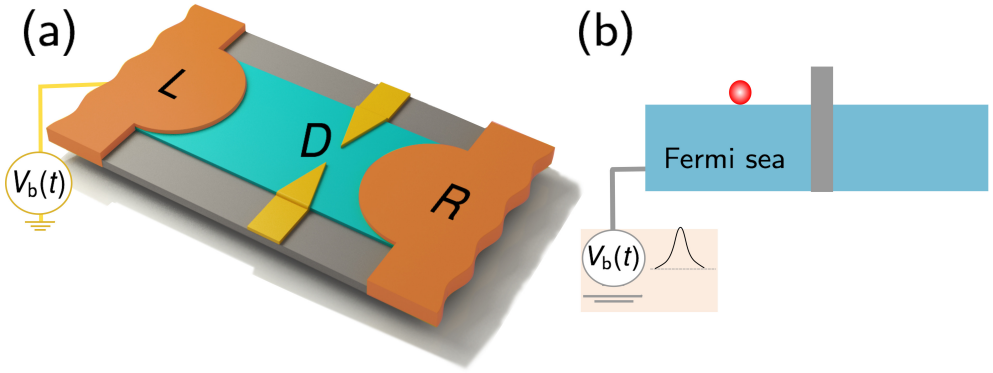

Figure 4.1: *(a) Sketch of a typical setup for the Lorentzian bias voltage consists of a coherent conductor (the green area) with a central QPC of transparency D (the yellow area). The conductor is connected to two reservoirs L and R (the orange area). Both reservoirs are kept at the same temperature, k_BT. By applying the Lorentzian-shaped, time-dependent bias voltage $V_b(t)$ to reservoir L, single electrons propagate along the coherent conductor. These electrons can be reflected or transmitted at the central QPC. (b) Creation of a Leviton onto the Fermi sea without any trace of additional electron-hole pairs.*

by using split gates. We consider a single channel with transmission D in the conductor which is created due to a high negative voltage in the gates. By applying a periodic Lorentzian voltage, $V_\mathrm{b}(t)$, to the reservoir L, single-electron excitations, which was named Levitons, are generated in the conductor. Mathematically, the expression for the periodic Lorentzian voltage has the form

$$V_\mathrm{b}(t) = \frac{V_0\mathcal{T}}{\pi}\sum_{j=-\infty}^{\infty}\frac{\sigma_\mathrm{lev}}{\left(t - t^e_\mathrm{lev} - j\mathcal{T}\right)^2 + \sigma^2_\mathrm{lev}}. \tag{4.1}$$

This Lorentzian pulse has the width of $2\sigma_\mathrm{lev}$ at half maximum and it is characterized by the emission time of t^e_lev within the period $\mathcal{T}$. The integer Faraday flux, $(e/h)\int_0^{\mathcal{T}} \mathrm{d}tV_\mathrm{b}(t)$, verifies that the Lorentzian pulse leads to an integer number of injected electrons. Here, we assume that exactly one electron in every period is emitted, thus

$$\frac{e}{h}\int_0^{\mathcal{T}} \mathrm{d}tV_\mathrm{b}(t) = \frac{eV_0}{h/\mathcal{T}} = 1. \tag{4.2}$$

Therefore, V_0 is defined as

$$V_0 = \frac{\hbar\Omega}{e}, \tag{4.3}$$

where $\Omega = 2\pi/\mathcal{T}$ is the driving frequency of the voltage. In the experiment conducted by Dubois and co-workers [9], the shortest possible Lorentzian pulse was 30 ps wide, with a driving period of $\mathcal{T} = 166$ ps. These experiments were conducted at a temperature of $T = 35$ mK. In Chap. 5, we explain different experiments that result in realization of the Leviton such as shot noise, the Hong-Ou-Mandel noise

correlator measurement and also tomographic noise measurement to reconstruct the quantum state.

Using the shot noise and the Hong-Ou-Mandel noise correlator measurement, the wavefunction probability of the Leviton both in a time domain and an energy domain can be found. Later, in another experiments [48, 49], the full wavefunction of the Leviton, the Wigner function[1] [96, 97], was reconstructed through tomographic noise measurement to characterize the purity of the emitted states.

The probability amplitude with which the emitted electrons from reservoir L propagate along the single channel is obtained by inserting Eq. (4.1) into Eq. (2.27) from Chap. 2, so that one finds

$$c_{\mathrm{L},n} = \begin{cases} -2\Omega\sigma_{\mathrm{lev}}\, e^{-n\Omega\sigma_{\mathrm{lev}}}\, e^{i(n+1)\Omega t_{\mathrm{lev}}} & n > -1, \\ -e^{-\Omega\sigma_{\mathrm{lev}}} & n = -1, \\ 0 & n < -1. \end{cases} \tag{4.4}$$

One can see that the emitted particles depend only on the transferred energy, $n\hbar\Omega$, and are independent of the incoming energy, E. We also require $\Omega\sigma_{\mathrm{lev}} \ll 1$, to ensure that the pulses are well-separated in time. Next, the electrons which propagate along the conductor impinge on the QPC with transmission probability D. The relation between the particles injected to the conductor and scattered those from the QPC is given by

$$S(E) = \begin{pmatrix} \sqrt{1-D(E)} & \sqrt{D(E)} \\ \sqrt{D(E)} & -\sqrt{1-D(E)} \end{pmatrix}. \tag{4.5}$$

Using Eqs. (4.4) and (4.5), we are able to calculate the transport quantities which were introduced in Sec. 2.5.2. This calculation is done in Paper I: by studying the impact of the generic properties of this SES on the transport quantities, the precision and the spectrum of the source can be characterized.

4.2 Slowly driven mesoscopic capacitor

Creating single particles in a quantum-confinement regime with a time-dependently driven mesoscopic capacitor has been first realized by Fève and co-worker [4, 14]. Taking advantage of the discrete energy spectrum due to confinement allows for obtaining the emission of particles one by one. This specific feature has been employed when using a mesoscopic capacitor as an accurate SES.

As it is shown in Fig. 4.2(a), the mesoscopic capacitor is realized in a 2DEG conductor in the quantum Hall regime. For this to happen, an external magnetic

[1] This function is the partial Fourier transform of the first order electronic correlation function which can reconstruct the quantum state of single electronic excitations, for more detail see Appendix B of Paper I.

field $B \approx 1.3$ T is applied perpendicularly to the 2DEG to create edge states, which are depicted in Fig. 4.2(a) by red lines (here we restrict the model to the single-channel case). This source is made of a confined region with a level spacing Δ which is coupled to the conductor through a QPC with transparency D_s from one side, and from the other side capacitively to the top-gate voltage.

By driving the time-periodic gate voltage, electrons can be emitted or absorbed. As it is shown in Fig. 4.2(b), by increasing the potential of QD, the energy level of the QD is moved above the Fermi level, and this leads to the emission of an electron. Then, by decreasing the potential, the energy level is brought back to its initial position, and thereby one hole leaves the dot, or in other words, the level gets occupied again by an electron. As a result, one electron and one hole are released per period into the edge state in the conductor but in well-separated manner. In the experiment in Ref. [4], the applied voltage is a sudden voltage step, and depending on the deriving amplitude, particles are emitted far above the Fermi level. In this experiment, the emission of electrons and holes was realized at driving frequencies of the order of 1 GHz, with the transparency of the QPC, D_s, being around 0.03 and the emission time below one nanosecond. Unlike that experiment, here we consider a sinusoidal voltage that excites particles around the Fermi level which leads to the generation of the Lorentzian pulse in time. The temporal pulses of the emitted particles (electron and hole in each period) are shown in Fig. 4.4 to compare with pulses from other sources.

Note that, the edge states can be used as electron wave guides in quantum optics with electrons, this has been used in various experiments [27, 49, 98–110], which are mentioned also in Chap. 5.

Now, we move on to describe this setup with the relevant scattering matrix. To do so, first we treat only the capacitor as a scatterer, then later, we add the QPC to the scatterer. The particles which are scattered from the capacitor, acquire a time-dependent phase due to the induced time-dependent potential, $U(t) = \delta U(t) + \bar{U}$, where $\delta U(t)$ denotes the ac component, and $\bar{U}$ is a dc component of the potential fixing the position of the energy levels. Also an energy-dependent phase due to the discrete level spectrum of the confined region, respectively. Therefore, the scattering matrix is constructed as [102]

$$S_\mathrm{cap}(t,E) = -\sqrt{1-D_\mathrm{s}} + D_\mathrm{s}\sum_{q=1}^{\infty}\left(\sqrt{1-D_\mathrm{s}}\right)^{q-1} e^{iqkL} e^{-i\frac{e}{\hbar}\int_{t-q\tau}^{t} dt' U_\mathrm{g}(t')}. \tag{4.6}$$

Here, q corresponds to the number of times an electron travels around in the capacitor before it is injected into the conductor at time t, where $\tau = m_e L/(\hbar k_\mathrm{F})$ is the time for an electron with mass m_e to make a single turn around the capacitor of length L.

We are interested in a regime where well-separated pulses of single electron and hole are emitted. For this reason, first, the adiabatic-response regime needs to be considered, where the potential changes slowly with respect to the average time

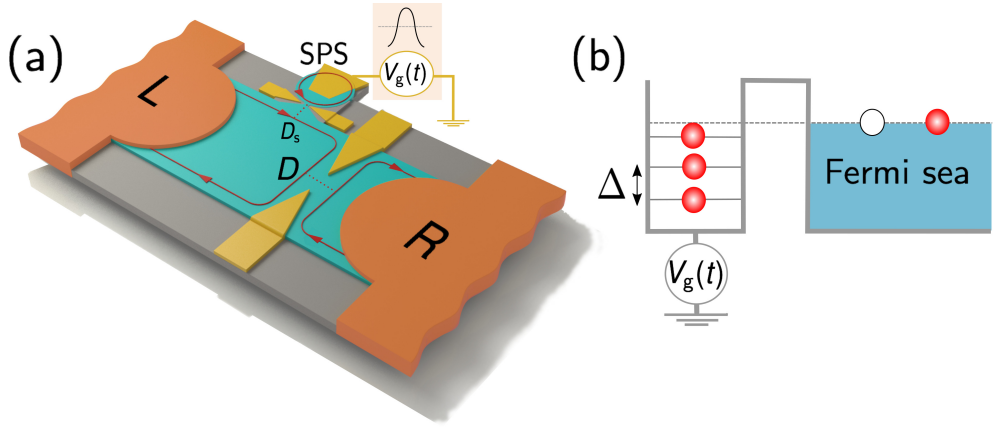

Figure 4.2: *(a) Sketch of the slowly driven mesoscopic capacitor setup. The single electron source (SES) consists of a mesoscopic capacitor with a time-dependently driven gate voltage $V_g(t)$. The capacitor is coupled to the edge state of a 2DEG through the QPC with transparency D_s. Single particles Injected from the capacitor propagate along an edge state (red lines with arrows) in the 2DEG. These particles can be reflected or transmitted by the central QPC with transparency D. (b) Principle of the single electron emission by the mesoscopic capacitor. It emits one electron/hole separately when an energy level of the QD resonates with the Fermi level of the reservoir. The level spacing of the capacitor is $\Delta = h/\tau$.*

that an electron spends in the capacitor. This assumption is valid if the relevant adiabaticity parameter is sufficiently small, i.e.,

$$\frac{\Omega\tau}{D_\mathrm{s}} \ll 1, \tag{4.7}$$

with the driving frequency Ω. The second condition is given by

$$\Omega\sigma_\mathrm{cap} \ll 1, \tag{4.8}$$

where $2\sigma_\mathrm{cap}$ is the temporal width of the emitted pulse. The above condition together with the third one,

$$k_\mathrm{B}T \ll |e\delta U|, \tag{4.9}$$

while $\bar{U} = 0$, guarantees the generation of a train of current pulses which are well-separated in time. In this regime, the scattering matrix of the mesoscopic capacitor can be expressed in terms of the frozen scattering matrix, Sec. 2.4.1, as (for more details see Appendix A.1)

$$S^{(0)}_\mathrm{cap}(t,E) = \frac{t - t^{(\mathrm{h})}_\mathrm{cap}(E) - i\sigma_\mathrm{cap}}{t - t^{(\mathrm{h})}_\mathrm{cap}(E) + i\sigma_\mathrm{cap}} + \frac{t - t^{(\mathrm{e})}_\mathrm{cap}(E) + i\sigma_\mathrm{cap}}{t - t^{(\mathrm{e})}_\mathrm{cap}(E) - i\sigma_\mathrm{cap}} \equiv S^{(0,\mathrm{h})}_\mathrm{cap}(t,E) + S^{(0,\mathrm{e})}_\mathrm{cap}(t,E), \tag{4.10}$$

where the scattering matrix is decomposed into the resonant emission of holes (h) and electrons (e) in the energy-dependent emission times $t^{(\mathrm{h})}_\mathrm{cap}(E)$ and $t^{(\mathrm{e})}_\mathrm{cap}(E)$,

respectively. The emission times and the width of the pulse in time, $\sigma_{\rm cap}$, are found to be

$$\begin{cases} t^{(\rm e)}_{\rm cap}(E) = \dfrac{E + e\bar{U}}{e\delta U\Omega}, \\ t^{(\rm h)}_{\rm cap}(E) = \dfrac{\mathcal{T}}{2} - t^{(\rm e)}_{\rm cap}(E), \end{cases} \quad \text{and} \quad \sigma_{\rm cap} = \frac{D_{\rm s}\hbar}{2e\delta U\tau\Omega}. \tag{4.11}$$

On the other hand, the scattering matrix (4.10) can equivalently be reformulated in terms of the time-dependent resonant energies $E^{(\rm h/e)}_{\rm res}(t)$:

$$S^{(0)}_{\rm cap}(t,E) = \frac{E - E^{(\rm h)}_{\rm res}(t) - i\Gamma}{E - E^{(\rm h)}_{\rm res}(t)(t) + i\Gamma} + \frac{E - E^{(\rm e)}_{\rm res}(t) - i\Gamma}{E - E^{(\rm e)}_{\rm res}(t) + i\Gamma} \equiv S^{(0,\rm h)}_{\rm cap}(t,E) + S^{(0,\rm e)}_{\rm cap}(t,E), \tag{4.12}$$

with

$$\begin{cases} E^{(\rm e)}_{\rm res}(t)(t) = e\delta U\Omega t, \\ E^{(\rm h)}_{\rm res}(t) = e\delta U\pi - E^{(\rm e)}_{\rm res}(t), \end{cases} \quad \text{and} \quad \Gamma = D_{\rm s}\frac{\hbar}{2\tau} = e\delta U\Omega\sigma_{\rm cap}. \tag{4.13}$$

In this representation, the width of an energy level of the capacitor, Γ, is accessible. This width is defined by the coupling between the capacitor and the conductor. A more general form of the scattering matrix $S^{(0)}_{\rm cap}(t,E)$ with the time-dependent resonant energy $E_{\rm res}(t)$, which is not linearized around the emission times, is provided in Appendix A.2.

Now, using Eq. (2.19), the scattering matrix in the energy domain is found to be

$$S_{\rm cap}(E_n,E) = \begin{cases} -2\Omega\sigma_{\rm cap}e^{-n\Omega\sigma_{\rm cap}}\mathrm{e}^{in\Omega t^{(\rm e)}_{\rm cap}(E)}, & n>0, \\ -2\Omega\sigma_{\rm cap}e^{n\Omega\sigma_{\rm cap}}\mathrm{e}^{in\Omega t^{(\rm h)}_{\rm cap}(E)}, & n<0, \\ \delta_{n,o}, & n=0. \end{cases} \tag{4.14}$$

As shown in Fig. 4.2, electrons emitted from the capacitor, propagate along the edge state, and they impinge on the central QPC with transparency D. These electrons can then be reflected back to reservoir L with the probability amplitude $\sqrt{1-D}$, or can be transmitted to reservoir R with the probability amplitude $\sqrt{D}$. The total scattering matrix, including the effect of scattering at the central QPC and the mesoscopic capacitor, can be written as

$$S(E_n,E) = \begin{pmatrix} \sqrt{1-D}\ S_{\rm cap}(E_n,E) & \sqrt{D}\ \delta_{n0} \\ \sqrt{D}\ S_{\rm cap}(E_n,E) & -\sqrt{1-D}\ \delta_{n0} \end{pmatrix}. \tag{4.15}$$

Inserting Eq. (4.15) in Sec. 2.5.1, we can calculate the transport quantities in this setup. Due to the discrete spectrum of the capacitor, these observables are strongly temperature-dependent, which is extensively studied in Paper I. Moreover, this setup is used in Paper II and IV as an illustrative example to confirm the feasibility of our detection schemes.

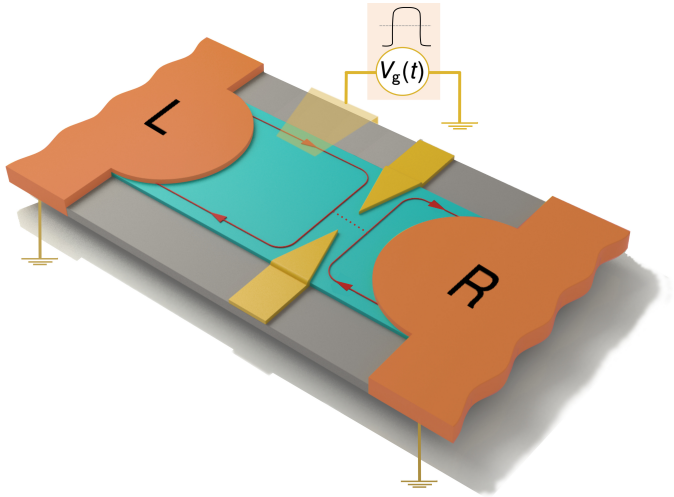

Figure 4.3: *Sketch of the setup where the edge state is locally and time-dependently modulated. The conductor is a 2DEG in the quantum Hall regime. Particles propagate ballistically along the edge state. The left upper edge state is locally modulated by applying a smooth-box potential $V_g(t)$ which leads to the emission of an electron and a hole per driving period.*

4.3 Local time-dependent edge-state modulation

Realization of SESs in the quantum Hall regime is important in the context of the quantum optics with electrons. Therefore, in Ref. [18], another way of generating single particles has been suggested in the same setup as the mesoscopic capacitor, but without any confinement region. Such a setup, i.e., open mesoscopic capacitor, has been studied theoretically [111] and experimentally [14], but, the trace of single particles has not been realized in these studies. However, in Ref. [18] it is shown that in such a setup, a particular shape of driving gate voltage is required to create quantized current pulses corresponding to single particles. The required voltage can be applied by a capacitively-coupled gate to the top-left edge state, as shown in Fig. 4.3 and it is given by

$$V_{\rm g}(t) = \frac{V_{\rm g}}{2\pi}\,{\rm Re}\left\{ i \ln\left[\frac{\sin\left(\Omega[t - t^{(\rm e)}_{\rm loc} + i\sigma_{\rm loc}]/2\right)}{\sin\left(\Omega[t - t^{(\rm e)}_{\rm loc} + i\sigma_{\rm loc}]/2\right)}\right]\right\}. \tag{4.16}$$

This smooth-box gate voltage shapes the injected current signal to well-separated pulses corresponding to emission of an electron and a hole. This has been shown in Fig. 4.4, and compared with other presented sources. The Floquet scattering matrix describing the region of the conductor which is affected by the gate voltage is given by

$$S_{\rm loc}(E_n, E) = e^{iE\tau_{\rm g}/\hbar} c_{{\rm g},n}. \tag{4.17}$$

Here, τ_g stands for the travel time of an electron passing through the gated region. The amplitudes $c_{g,n}$ are defined analogously to Eq. (4.4), with

$$c_{g,n} = \int_0^{\mathcal{T}} \frac{dt}{\mathcal{T}} e^{-in\Omega t} c_g(t) \quad \text{and} \quad c_g(t) = e^{i\frac{e}{\hbar}\int_{t-\tau_g}^{t} dt' \delta V_g^{\text{eff}}(t')}. \tag{4.18}$$

Above, $\delta V_g^{\text{eff}}(t')$ is the internal potential generated in the conductor within the interaction region. The relation between this potential and externally applied gate potential, according to Ref. [18] in the adiabatic-response limit, is given by

$$\delta V_g^{\text{eff}}(t) = \frac{C_\mu}{C_q} \delta V_g(t), \tag{4.19}$$

where, $C_\mu = C^{-1} + C_q^{-1}$ denotes the total electrochemical capacitance of the purely electrostatic capacitance, C, connected in series with a quantum capacitance, $C_q = \tau_g e^2/h$. With this assumption and using Eq. (4.16), the coefficient $c_{g,n}$ is obtained as

$$c_{g,n} = \begin{cases} -2\Omega\sigma_g\, e^{-n\Omega\sigma_g}\, e^{in\Omega t_{\text{loc}}^{\text{e}}} & n > 0, \\ 1 & n = 0, \\ -2\Omega\sigma_g\, e^{n\Omega\sigma_g}\, e^{in\Omega t_{\text{loc}}^{\text{h}}} & n < 0. \end{cases} \tag{4.20}$$

Consequently, the total scattering matrix of the system which describes the locally modulated edge state and the central QPC is given by

$$S(E_n, E) = \begin{pmatrix} \sqrt{1-D}\; e^{iE\tau_g/\hbar} c_{g,n} & \delta_{n0}\sqrt{D} \\ \sqrt{D}\; e^{iE\tau_g/\hbar} c_{g,n} & -\delta_{n0}\sqrt{1-D} \end{pmatrix}. \tag{4.21}$$

The properties of this SES can be studied by inserting the scattering matrix introduced above, Eq. (4.21), into the relevant expressions for the transport quantities, discussed in Sec. 2.5.1. This part of the analysis is carried out in Paper I. As a result, application of the smooth-box driving potential in the adiabatic response regime leads to the emission of well-separated pulses of an electron and a hole and consequently, the emission scheme of this setup becomes comparable with the two other mentioned setups. In the following discussion section of this chapter, we argue this comparison between the different setups.

4.4 Discussion

In this chapter, we have introduced the three different SESs and show how to model them with their associated scattering matrix. The difference between them stems from the characteristics of their driving voltage, and in addition, the second source (mesoscopic capacitor), works in a quantum-confinement regime, which is not the case for the other two sources. However, as a common feature, all three sources only minimally excite the Fermi sea.

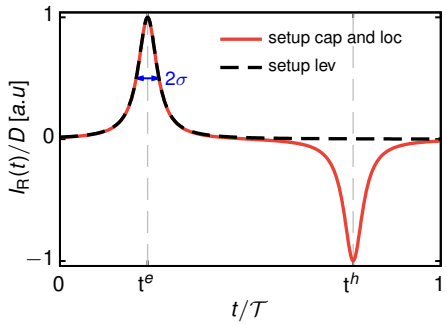

Figure 4.4: *The electron-current pulses that are emitted from the three SESs discussed in this chapter. The red solid line indicates the slowly driven mesoscopic capacitor (setup cap) and the local time-dependent edge-state modulation (setup loc) whereas the black dashed line corresponds to the Lorentzian-shaped bias voltage (setup lev). The setup cap and loc emit one electron pulse at time t^e and one hole pulse at time t^h, while the Lorentzian-shaped bias voltage leads to emission of only one electron pulse at time t^e. The width of the pulses in the three SESs are given by σ.*

In Fig. 4.4, the electron-current pulses emitted by these SESs are shown at low temperatures. In this figure, we consider a same pulse width for all sources, i.e., $\sigma_{\rm cap} = \sigma_{\rm lev} = \sigma_{\rm loc} \equiv \sigma$. Analogously, we assume the emission times of the capacitor and the local gate as $t^e_{\rm cap} = t^e_{\rm loc} \equiv t^e$ and $t^h_{\rm cap} = t^h_{\rm loc} \equiv t^h$, and the emission time of the Leviton as $t^e_{\rm lev} \equiv t^e$.

As it is shown in Fig. 4.4, the electron-current pulses from different setups are similar. The difference comes from the fact that the mesoscopic capacitor setup and the local gate setup create an electron and a hole current pulse, whereas the Lorentzian bias voltage setup only emits an electron pulse. The other difference which is not covered here is the temperature dependency of the signals. This is extensively discussed in Paper I and where we demonstrate that the electron-current pulses emitted by the driven capacitor become strongly dependent on the other parameters, such as the energy emitted per pulse, ϵ, level broadening, Γ and temperature.

So far, we have gained the required background on the SESs and their description in the scattering matrix context, which is required to derive transport quantities. In general, information about the type and the number of injected particles from SESs are encoded in the transport quantities. In addition, the impact of the temperature on the particle emission is also reflected in them which are studied thoroughly in Paper I. Now, we can move on to the next chapter where these observables are employed as a spectroscopy tool to characterize the SESs.

5 Characterization of on-demand electron sources

In the previous chapter we discussed three different schemes of generating single-electron pulses on demand. In Paper I and IV, we use transport and thermoelectric quantities to gain insight into the properties of single electron sources (SESs). Then, from the experimental point of view, the relevant question arises how to access these properties in practice. In Paper II we propose a novel detection scheme to read out charge and energy noises via frequency-dependent temperature and electrochemical-potential fluctuations in a probe reservoir. On the other hand, in Paper IV we use an energy-dependent barrier to detect the spectral current through thermoelectric effects. In this chapter, we overview other related works on how to detect, and further, how to characterize such SESs and compare them with our detection schemes.

5.1 Time-resolved charge current

Generation of single particles in SESs occurs due to time-dependent driving, therefore the time-resolve charge current is of interest. This quantity is in general difficult to detect. However, in the first experiment that was performed by Fève and co-workers [4], the time-resolved charge current has been ideally measured in the mesoscopic capacitor setup which worked as a SES.

In that case, as it is shown in Fig. 5.1(a), the square-shaped driving potential was applied to the mesoscopic capacitor via capacitive coupling of the capacitor to a gate. By considering a large top gate capacitance, and bearing in mind that the Coulomb energy is small and thereby negligible, the total charging energy is then proportional only to the level spacing of the capacitor levels, Δ. The escape time of the electron due to the coupling of the capacitor to the conductor through a QPC with transparency D, is given by $\tau = h/D\Delta$. The escape time is of the order of nanoseconds which implies that the detection of a single charge is experimentally difficult. However, they resolved this problem by making D very small which leads to longer escape time. Furthermore, in order to get a measurable current, increasing signal-to-noise ratio, a statistical average over many individual events was done by applying a periodic square-shaped voltage, and as a result, the sequence of single particles (electrons and holes) was emitted. Finally, the

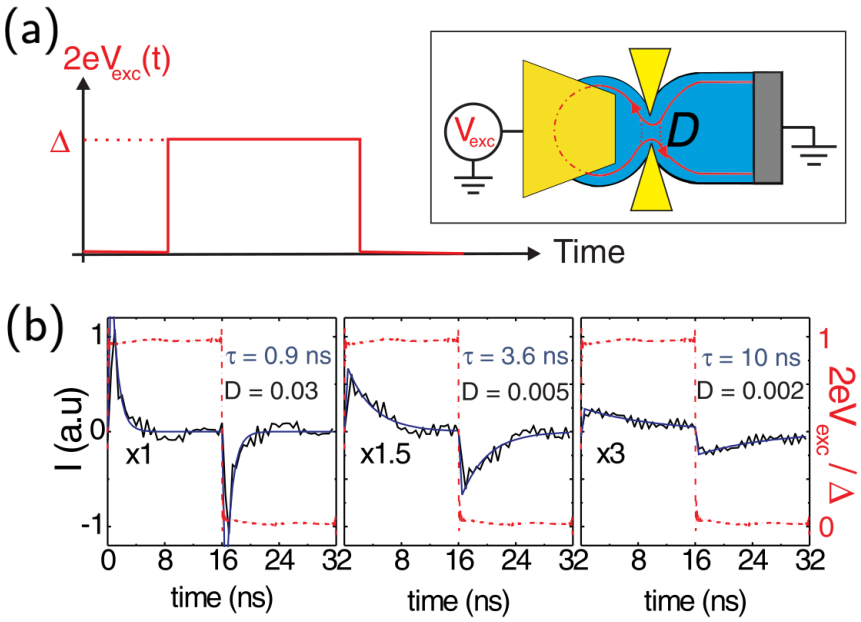

Figure 5.1: *(a) Capacitor coupled from one side to the conductor through the QPC with transparency D, and from the other side capacitively connected to the gate. (b) The time-resolved charge current for a period of $T = 32$ ns for three different probability transmissions D. The amplitude of the voltage was of the order of level spacing, $V_{exc} \sim \Delta$. The relaxation time τ was extracted from an exponential decay (blue curve). Figure is taken from Ref. [4].*

time-resolved charge current was measured by performing the statistical average over many individual events.

As it is illustrated in Fig. 5.1(b), the average over all emissions reconstructs the exponential charge current in a time domain. The decay time is defined by relaxation time τ which is a function of D. It essentially means that the probability of transmission plays an important role: At very small D, the escape time increases and the quantized current is lost. On the other hand, in the limit of the large transparency, $D \sim 1$, quantum fluctuations occur. In this experiment, it was shown that by choosing $D = 0.03$, the current in each half-period decayed to zero, and thus, it was possible to see the effect of single particles.

Note that this technique is only possible for slowly time-dependent driving since the time-resolution of the detector is limited. At the same time the slow driving reduce the magnitude of the current, see the right-most plot in Fig. 5.1(b), requiring large measuring time.s

In paper I, we calculate the time-resolved charge current for three different sources, Chap. 4, in all temperature regimes. We demonstrate that, in the setup based on the slowly driven mesoscopic capacitor, the emitted signal is modified at high temperatures which is related to the energy-dependent scattering matrix. We expect that with the technique above, the predicted temperature-dependent time-resolved charge current can be measured.

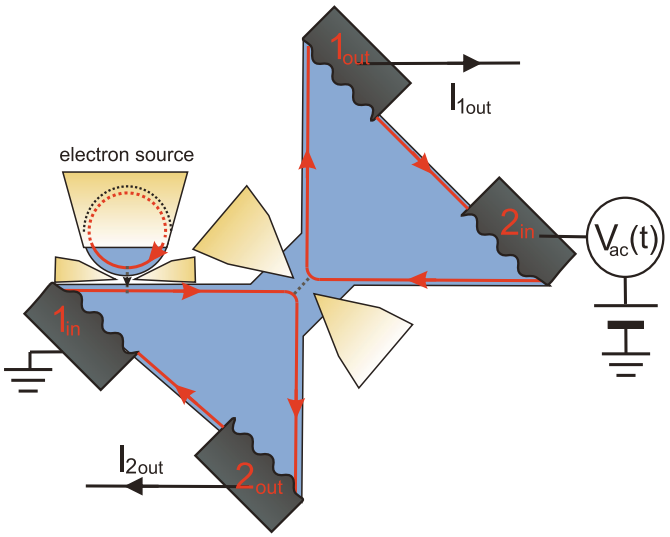

Figure 5.2: *Sketch of a four-terminal setup in the quantum Hall regime. Output contacts 1 and 2 are used to detect noises. A single-electron source based on the mesoscopic capacitor is placed on the incoming channel 1, while a sinusoidal voltage is applied to the Ohmic input contact 2. Figure is taken from Ref.[101].*

In general, this technique, which is realization of a coherent SES based on a mesoscopic capacitor in the quantum Hall regime, paved the way for new experiments in quantum optics with electrons, such as, Mach-Zehnder interferometer [27, 98–100], using two sources for Hanbury Brown-Twiss (HBT) [49, 101–104], Hong-Ou-Mandel interferometer(HOM) [105–110], and electron entanglement in multi-lead conductor.

5.2 Low-frequency charge-current noise

ore than two decades passed since it was noticed that noise, which comes from the fluctuations, despite its disruptively sounding name, is a very practical quantity. In fact, in the mesoscopic physics, noise is used as an additional tool to learn about the properties of the conductor [74]. For instance, it is employed to identify the fractional charges in the integer quantum Hall effect regime via Fano factor [102].

In the context of SESs characterization, using noise is an important tool that provide us with valuable insight into the precision of the source. To be more specific, measuring charge-current noise gives access to the number of emitted particles, including neutral electron-hole pair excitations, which indicates the precision of the source [112, 113]. As an example in Ref. [24], the number of generated electron-hole pairs for different types of time-dependent bias voltage were investigated through measuring the noise. In the course of this studies, a predicted Leviton [15] with minimal electron-hole pairs in Refs. [9, 25] experimentally was identified.

Apart from these fundamental properties, the analysis of noise can also be used in more complex setups to identify other phenomena associated with properties of SESs, such as quantum tomography. For example, in an HBT setup, in analogy to quantum optics, using noise measurements, one can demonstrate that the quantum tomography allows for the reconstruction of the quantum state of emitted particles [101, 114]. Let us explain this technique by exploring Ref. [101]. As it is shown in Fig. 5.2, a four-terminal setup with central QPC was considered. The SES was placed on the incoming channel 1 and sinusoidal voltage was applied to the input contact 2. When the emitted particles from two channels collided on a QPC, the output current correlator encodes information on the emitted particles from the source and ac voltage. In this setup, by finding a suitable ac voltage, having the same frequency as the source, and measuring the zero-frequency current correlator, it became possible to determine single-particle coherence of the SES. In fact, this experiment led to the reconstruction of the temporal and spatial single-particle coherence. Similar technique was later used to reconstruct the full wavefunction of the Leviton which characterized the purity of the emitted states [48, 49].

In Paper I, we theoretically study the low-frequency charge-current noise in a vast range of temperatures for the three distinct sources which are described in Chap. 4. We expect that this transport quantity can be measured directly in our (proposed) setup. However, in Paper II, we suggest a setup which allows for the indirect detection of the low-frequency charge-current noise by measuring finite frequency electrochemical potential correlators in a probe.

5.3 Energy-resolved charge current

Since electrons carry not only charge, but also energy [26, 27], the energy distribution of the emitted particles is a relevant parameter to characterize the SES. In principle, the energy distribution is accessible through energy-resolved charge currents. In Ref. [102], the similar HBT setup, Fig. 5.2, is used to measure noise, as it has been discussed in previous section. However, here, noise measurements are utilized not only for the precision, but also for probing energy distribution of emitted particles. For this purpose, a thermal bias, instead of the ac voltage, is applied to the input contact 2. Then, antibunching of low energy excitations with thermal excitations is observed and used to probe the energy distribution of emitted particle.

In other experimental studies [50, 51, 115], it has been shown that the energy distribution can also be measured with the help of an energy-dependent detection barrier. Following Re.[50], as it is shown in Fig. 5.3(a), single emitted particles impinge on the energy-dependent barrier, and then, they are reflected back or transmitted to the output channels. This is also shown in Fig. 5.3(b) with the potential profile of the pump and detector. In this study, a reflected current

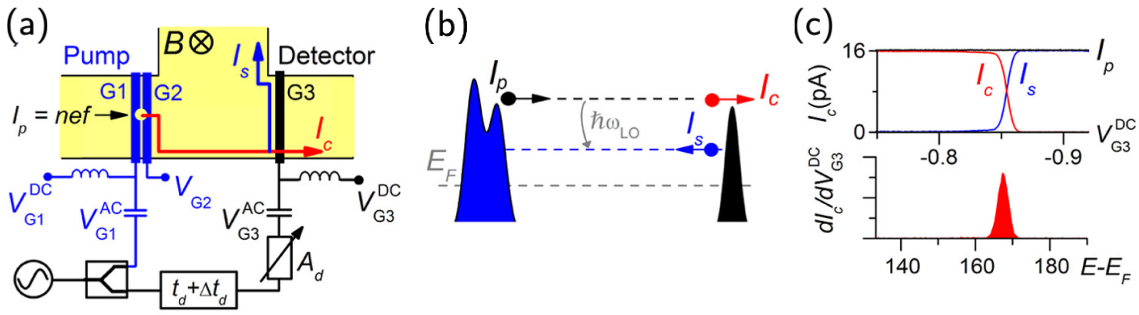

Figure 5.3: *(a) Sketch of an energy-detector barrier: Single particles generated by dynamical QDs are reflected by or transmitted through the energy-dependent barrier. The device is divided into the pump and the detector. (b) The reflection and transmission of particles is also shown in th potential profile. (c) A reflected and transmitted current were measured with ammeters, which were of the order of* 16 *pA, and next the conductance with respect to the gate voltage was reconstructed. Figure is taken from Ref. [50].*

I_s, a transmitted current I_c, and consequently, the gate conductance dI_c/dV_{G3}^{DC} were measured. As it can be seen in the conductance plot in Fig. 5.3(c), the energy-resolved charge current becomes accessible. In fact, by measuring the conductance, one gains insight into the energy distribution of the emitted particles. In the aforementioned experiments, the SES under investigation emitted particles far above the Fermi sea, meaning that for $E_f = 10$ meV the energy of emitted particle was around 170 meV. However, in the case of the SESs that we are interested in, namely, those that minimally excite the Fermi sea, the temperature indeed becomes an important factor. In paper IV, along the same line as presented experiments, we propose an energy-selective detection scheme to read out the energy-resolved charge current which, in turn, allows for characterization of the SESs. We suggest that measuring conductance with respect to the bias voltage (not the gate voltage) leads to reading out the spectral current. Moreover, we show that upon applying thermal bias, other measurable thermoelectric quantities can also be used to read out this quantities.

5.4 Heat current and heat-current noise

Another way to access some of the energetic properties of the emitted particles is through the heat current and the heat-current noise. Many theoretical works have been devoted to the study of these quantities and their possible yield in finding further information about the spectral properties of the setup of interest [36, 38–40, 116, 117]. There are several experimental proposals to measure, particularly, the heat-current noise. In Ref. [38], for example, it is shown that when the source is voltage-bias driven, the heat-current fluctuations can be read out by detecting

power fluctuations.

In Paper II, we propose a setup to read out the charge-current noise, and more importantly, the heat-current noise, by measuring electrochemical potential and temperature correlators [43, 44, 118]. The feasibility of the experiment relies on the fact that fast temperature measurement techniques are available nowadays [119]. The fast and ultra-sensitive thermometer introduced in Ref. [119], is based on a normal metal-insulator-superconductor probe in an LC resonant circuit. This thermometry provides 90 $\mu\mathrm{K}/\sqrt{\mathrm{Hz}}$ thermometry in 10 MHz. It means that the fast thermometry gives access to the temporal statistical variation in mesoscopic structure by measuring the temperature over timescales shorter than the thermal relaxation time. Moreover, fast thermometry is of key importance in the thermodynamic studies. For instance, in Refs. [120, 121], this technique has been used to measure quantum thermal conductance. These findings have served as a motivation in Paper IV, wherein we study the thermal conductance and other thermoelectric coefficients as a characterization tool to learn about the SESs.

As pointed out above, there are many theoretical and experimental works on characterization and detection of single-electron emissions. Proper understanding of the SESs that provide such emissions is important for the current, and also for future applications of the mesoscopic physics. In this chapter, we have summarized some of the present and possible future investigations on the on-demand SESs. We have also shown the relevance of our work by establishing a connection between the appended papers and other published studies.

6 Overview of the papers

This chapter summarizes motivation, approach and outcome of papers that constitute the research of this thesis.

6.1 Paper I

In this paper, we analyze the emission of single-particle pulses from three distinctive types of on-demand single-electron sources whose common feature is that they only minimally excite the Fermi sea, Chap. 4. These sources are: a slowly driven mesoscopic capacitor, a Lorentzian-shaped time-dependent bias voltage, and a local gate-voltage modulation of a quantum Hall edge state. In this context, observables (such as time-resolved charge and energy, as well as spectral currents, or zero-frequency correlators of charge and energy currents) can serve as a spectroscopic tool for acquiring additional information on spectrum and accuracy of the injected particles.

We show that in a simple setup, consisting of a single-electron source and a QPC, the behavior of the observables can be fully described by a small set of experimentally relevant and theoretically understandable parameters, namely averaged energy emitted per pulse ε, level broadening Γ (relevant in the capacitor setup created by confinement) and temperature T. Using this set of parameters, we clearly identify the behavior of these differently operated sources in a large temperature interval, and thereby, provide an extensive overview of the characteristics of single-particle sources visible in the observables. We find out that the differences in the transport quantities between the sources at low temperature stem from the number and the type of the emitted particles. Furthermore, at high temperatures, we see that time-resolved currents are strongly temperature-dependent in the mesoscopic capacitor source due to the discrete spectrum, whereas in the other two sources they remain unchanged.

6.2 Paper II

In this paper, we theoretically propose an experimental method that allows for the extraction of information about transport properties of mesoscopic and nanoscale systems (as studied in Paper I), through measuring macroscopic fluctuations. We put forward a setup for the detection of fluctuating charge and energy currents,

as well as their correlations, generated by an arbitrary time-dependently driven electron source. More specifically, we demonstrate that these fluctuations should be accessible through the detection of macroscopic fluctuations of temperature and electrochemical potential in a probe contact.

First, we explain in detail the underlying physical mechanism of the proposed setup. Next, we discuss the feasibility of our detection scheme for a single-electron source based on a mesoscopic capacitor in the quantum Hall regime (explained in Paper I). We give an overview of different, experiment-related aspects that should be taken into account when optimizing the proposed detection scheme. In this respect, one important quantity to be investigated is heat current noise. We find out by choosing proper tunable parameters such as phonon coupling of the probe, transmission probability of the QPC and driving frequency, that the desired signal is not obscured by backaction effects of the measurement. Such a signal corresponds to the correlator of temperature fluctuations of the order of 10^{-4} K/$\sqrt{\text{Hz}}$ which is possible to measure with present experimental techniques. Therefore, we conclude that the proposed temperature fluctuation measurement gives direct access to the heat current noise from the source.

6.3 Paper III

In this paper, we theoretically investigate the operation of a QPC with an energy-dependent transmission function as a thermoelectric heat engine. Note that, we simply consider a two-terminal setup with a central QPC different from the other papers: in the absence of any kind of time-dependent source. We allow for arbitrary smoothness of the step-like function of energy in QPC transmission probability, and consider both linear and non-linear heat engine operation. We review and extend previous analyses of power production and efficiency. Besides efficiency and power, we suggest to consider the fluctuations to optimize the performance of a small system. This is different with macroscopic heat engine where fluctuations plays no role. We analyze the trade-off between a desired large power output, high efficiency and small fluctuations in the operation of heat engines in the context of Thermodynamic Uncertainty Relations (TURs).

First, we analyze the influence of the smoothness of the transmission probability on the behavior of output power and efficiency. We find out that reaching the maximum output power and efficiency requires the non-linear transport regime. By adding power fluctuations, we investigate a combined quantifier which is bound by TUR and we call it, TUR-coefficient. We show that this quantity is maximized in the linear response regime which corresponds to the regime of high efficiency but low output power. This result indicates how the fluctuation change the regime in which the QPC has optimized performance.

6.4 Paper IV

In this paper, we investigate an energy-selective detector with time-dependently driven single-electron sources for different possibilities in spectroscopy. The two-terminal setup with energy-dependent QPC is brought out of equilibrium linearly by thermal and voltage biases, resulting in thermoelectric effects in the conductor as is shown in Paper III. By adding an arbitrary time-dependently driven electron source, screening effects due to charge-pileup at the QPC become visible and modify the thermoelectric response coefficients. We discover that the screening effects together with time-dependent source opens up for two different experimental proposals: First, measuring modifications of thermoelectric coefficients due to the screening effects give access to the energetic properties of emitted particles. Second, using well-established single-electron sources as probes can sense unexplored (quantum) screening effects.

We find out that depending on the shape of the energy-selective transmission of the QPC, the modified electrical conductance, G_s, thermal conductance K_s and thermoelectric coefficients, $L_\mathrm{s}, M_\mathrm{s}$, can be proportional to the charge and heat currents and also spectral currents that purely come from the SES. In order to access these modifications, one has to subtract the conductances and thermoelectric coefficients when the source is switched off from results of the measurements with a working source. Importantly we show that, although the modified electrical conductance G_s and thermoelectric coefficient L_s stem from the potential- and temperature-bias induced screening properties, respectively, but, they carry the same information from the source. The same story stands for K_s and M_s. Thus, since we can employ a source as a probe and measure G_s and L_s, we directly get access to potential- and temperature-bias induced screening properties. In particular, this novel technique allows to detect the screening effects due to temperature which have not been observed so far.

7 Summary

This thesis and its appended papers study and discuss various aspects of the characterization of different types of time-dependently driven single-electron sources (SES). We show how the properties of SESs are reflected in transport observables such as charge and energy currents, and their corresponding zero-frequency correlators The latter one is accessible by introducing a quantum point contact (QPC), acting as a beam splitter, to the respective setup. These quantities can hence serve as spectroscopic tools to characterize SESs. Moreover, we provide proposals on how to read out these transport quantities experimentally.

We are specifically interested in three distinctive types of sources: a coherent conductor with a time-dependent Lorentzian-shaped voltage-bias driving, a gate-voltage driven mesoscopic capacitor in a quantum Hall conductor, and a quantum Hall edge state locally modulated by a smooth-box shaped gate voltage. These sources differ in the characteristics of time-dependent driving potential, and in the degree of particle confinement in the driven conductor. On the other hand, their common feature is that they only minimally excite the Fermi sea. These sources are introduced in Chap. 4. In order to derive the relevant transport observables, in a two-terminal setup with the mentioned SESs, we employ a scattering matrix approach, which is introduced in Chap. 2.

In Paper I, we have specifically analyzed how the transport properties of different SESs differ. We show that this behavior can be described by a small set of relevant parameters in a large temperature interval. These parameters include the averaged energy emitted per pulse, the energy width of the capacitor levels and the temperature. We find out that at low enough temperature, the three sources essentially emit the same electron-current pulses except for the first source that only emits an electron rather than emission of electron and hole, which is the case for the other two sources. Furthermore, we show that at high temperature, due to the discrete spectrum of the capacitor, transport quantities are strongly temperature-dependent.

Building upon this study of transport quantities as a spectroscopy tool for SESs, the rest of our work is focused on how these observables become accessible experimentally. This is particularly relevant for heat transport and energy-resolved transport which has not received much attention as compared to charge-related observables. In Chap. 5, we explain and review briefly the previous experimental works and proposals on the detection of transport quantities to learn about SESs. Furthermore, we address our proposed setups for the detection of the dis-

cussed transport quantities. In Paper II, we show that fluctuating charge and energy currents, as well as their correlations, should be accessible through the detection of macroscopic fluctuations of temperature and electrochemical potential in a floating probe contact. In Paper IV, we suggest an energy-dependent detection setup to read out energy distribution of the emitted particle through spectral current measurement. The investigations in these two papers, are based on the concrete example of a quantum Hall setup with a time-dependently driven mesoscopic capacitor acting as an SES.

For the scope of Paper IV, we use the introduced QPC as an energy-selective barrier. When applying a thermal and voltage bias across the QPC, is shown a thermoelectric response due to the energy-dependent transmission become noticeable in this system which is discussed in In Chap.3. This motivated us to take an intermediate step and, regardless of the SES characterization, we here study the QPC setup as a thermoelectric device. Therefore, in Paper III we investigate the QPC setup as a heat engine and study how to optimize the performance of the system. In this paper, we define a new performance quantifier using the trade-off between efficiency, output and power fluctuation which are restricted due to the so-called thermodynamic uncertainty relations.

Coming back to the energy-selective detection scheme in Paper IV, we show that combining a weak thermal and voltage bias with time-dependent driving, results in screening effects which are due to the accumulated charge in the conductor, is addressed In Chap.3. This effect leads to a shift of the QPC potential, and as a consequence modifies the linear thermoelectric response coefficients in the presence of the SES. Based on this, the suggested setup in Paper IV, offers different aspects of spectroscopy, both within but even beyond the initial scope of this work. First, we show that the energy distribution of emitted particles can be read out by measuring the modified thermoelectric response quantities. However, this interplay between screening and time-dependent driving also allows for a compliantly different, novel type of spectroscopy: we show that the screening effects are sensed by using a well-established SES as a probe.

7.1 Outlook

To conclude, we briefly discuss possible future directions of research arising from this work.

In the context of the SESs characterization, another relevant quantity to study is the first-order electronic correlation function, the Glauber function [46], which can be studied from the so-called Wigner function [96, 97]. In Paper I, we mention that the time-resolved charge current and the spectral current are two different marginals of the Wigner function. There, we also derive a general expression for the Wigner function and find out this quantity can as well be described by the same small set of parameters mentioned above. However, the temperature

dependence and also negativities of the Wigner function still have to be studied extensively for the three different SESs.

The proposed detection schemes in this work can be extended by considering an energy-dependent barrier, studied in Paper IV, in an open circuit introduced in Paper II. In this scheme, one can analyze the electrochemical potential and temperature, induced either by a thermal bias or a SES, in an energy-selective probe. These measurable quantities are expected to broaden the information accessible from spectroscopy.

Finally, Paper III, which is partially outside the initial scope of this work, leads to many open questions in stationary thermoelectrics that require further studies. In the context of the heat engine, it is intriguing to study performance quantifiers for other conductors with different energy-selective function [122] and compare it with the result of the QPC setup. Additionally, the question of how to quantify the QPC and other energy-dependent barriers, which are operated as refrigerators [57, 58], is not yet fully answered.

Appendices

Appendix A

Scattering matrix of the slowly driven mesoscopic capacitor

In the slowly time-dependent driven regime, the scattering matrix of the mesoscopic capacitor can be expressed in terms of the *frozen* scattering matrix. Here we derive this scattering matrix in terms of the resonant time and energy. The *frozen* scattering matrix, obtained from the lowest-order contribution in the driving frequency, is given by (details of the derivation can be found in Licentiate thesis. [71] and Refs. [77, 123]),

$$S^{(0)}(t,E) = e^{i(\gamma+\theta)}\frac{\sqrt{1-D_\mathrm{s}} + e^{i\phi(t,E)}e^{i(\gamma-\theta)}}{1+\sqrt{1-D_\mathrm{s}}\,e^{i\phi(t,E)}e^{i(\gamma-\theta)}}, \tag{A.1}$$

where the phase $\phi(t,E) = \Big[E + eU(t)\Big]\tau/\hbar + \Delta\phi$, consists of both the energy- and time-dependent parts, as well as a possible constant component $\Delta\phi$. Here, $\gamma+\theta$ is the overall phase of the scattering matrix, and $\gamma-\theta$ can be absorbed into $\Delta\phi$. The driving potential takes the form:

$$U(t) = \bar{U} - \delta U\sin(\Omega t). \tag{A.2}$$

Now, we assume that $D_\mathrm{s} \ll 1$, which is relevant for obtaining well-separated levels. This allows one to use the expansion $\sqrt{1-D_\mathrm{s}} \approx 1 - D_\mathrm{s}/2$, to perform a resonant expansion around $\phi_\mathrm{res}(t,E)$, with $\exp\Big[i\phi_\mathrm{res}(t,E)\Big] = -1$. It follows:

$$e^{i\phi(t,E)} \approx e^{i\phi_\mathrm{res}(t,E)} + ie^{i\phi_\mathrm{res}(t,E)}\Big[\phi(t,E) - \phi_\mathrm{res}(t,E)\Big] = -1 - i\Big[\phi(t,E) - \phi_\mathrm{res}(t,E)\Big]. \tag{A.3}$$

A.1 Scattering matrix written in terms of energy-dependent emission times

The phase, Eq.(A.3) can be expanded around the emission time,

$$\phi(t,E) - \phi_\mathrm{res}(t,E) \approx \Big[t - t_\mathrm{res}(E)\Big]\frac{\partial\phi(t,E)}{\partial t}\bigg|_{t=t_\mathrm{res}(E)}. \tag{A.4}$$

As a result, one obtains

$$S_{\mathrm{cap}}(t,E) = e^{i(\gamma+\theta)}\left\{\frac{t-t_{\mathrm{res}}^{(\mathrm{h})}(E)-i\sigma(E)}{t-t_{\mathrm{res}}^{(\mathrm{h})}(E)+i\sigma(E)}+\frac{t-t_{\mathrm{res}}^{(\mathrm{e})}(E)+i\sigma(E)}{t-t_{\mathrm{res}}^{(\mathrm{e})}(E)-i\sigma(E)}\right\}, \tag{A.5}$$

with

$$\begin{cases} t_{\mathrm{res}}^{(\mathrm{e})}(E) = \dfrac{1}{\Omega}\arcsin\left(\dfrac{E+e\bar{U}}{e\delta U}+\dfrac{\hbar}{\tau e\delta U}\left[\Delta\phi+\Gamma-\theta-\pi\right]\right), \\ t_{\mathrm{res}}^{(\mathrm{h})}(E) = \dfrac{\mathcal{T}}{2}-t_{\mathrm{res}}^{(\mathrm{e})}(E), \end{cases} \tag{A.6}$$

and

$$\sigma_{\mathrm{cap}}(E) = \frac{D_{\mathrm{s}}\hbar}{2e\delta U\tau\Omega}\cdot\frac{1}{\sqrt{1-\left(\frac{E+e\bar{U}}{e\delta U}+\frac{\hbar}{\tau e\delta U}\left[\Delta\phi+\Gamma-\theta-\pi\right]\right)^2}}. \tag{A.7}$$

Importantly, note that the term in square brackets can be canceled by adjusting the global phase.

Finally, it should be emphasized that the scattering matrix (4.10) is obtained from Eq. (A.5) by expanding the resonant (emission) times $t_{\mathrm{res}}^{(\mathrm{e/h})}(E)$ and the temporal width $\sigma(E)$ with respect to $|(E+e\bar{U})/(e\delta U)| \ll 1$,

$$\arcsin\left(\frac{E+e\bar{U}}{e\delta U}\right) \approx \frac{E+e\bar{U}}{e\delta U} \qquad \text{and} \qquad \frac{1}{\sqrt{1-\left(\frac{E+e\bar{U}}{e\delta U}\right)^2}} \approx 1. \tag{A.8}$$

In Chap 4, $t_{\mathrm{res}}^{(\mathrm{e/h})}(E)$ is replaced by $t_{\mathrm{cap}}^{(\mathrm{e/h})}(E)$,

A.2 Scattering matrix written in terms of time-dependent resonant energies

Following the previous section, one can expand the phase around the resonance energy rather than time, thereby we have

$$\phi(t,E)-\phi_{\mathrm{res}}(t,E) \approx \left[E-E_{\mathrm{res}}(t)\right]\left.\frac{\partial\phi(t,E)}{\partial E}\right|_{E=E_{\mathrm{res}}(t)}. \tag{A.9}$$

Then, by inserting this approximation in Eq. (A.1) and following an analogues argumentation as above, one obtains

$$S_{\mathrm{cap}}(t,E) = \frac{E-E_{\mathrm{res}}(t)-i\Gamma}{E-E_{\mathrm{res}}(t)+i\Gamma}, \tag{A.10}$$

with

$$\Gamma = D_{\mathrm{s}}\frac{\hbar}{2\tau} \quad \text{and} \quad E_{\mathrm{res}}(t) = -eU(t) - \frac{\hbar}{\tau}\Big[\Delta\phi + \gamma - \theta - \pi\Big]. \tag{A.11}$$

Recall also that $U(t) = \delta U(t) + \bar{U}$, and we assume the driving given by Eq. (A.2), and we consider $\bar{U} = 0$.

Finally, it must be noted that the scattering matrix (4.12) is obtained from Eq. (A.10) by linearizing the resonance energy $E_{\mathrm{res}}(t)$ around the emission times.

Appendix B

Thermoelectric coefficients of the QPC with step function transparency

In this appendix we derive thermoelectric coefficients, Eqs. (3.12) for the QPC with step function transmission, $D(E) = \Theta(E - E_0)$ which are given by

$$G = \frac{e^2}{h} f_0(E_0), \tag{B.1}$$

$$L = -\frac{M}{T_0} = \frac{e}{h}\frac{1}{T_0}\Big[\epsilon(f_0(E_0) - 1) - k_{\mathrm{B}}T_0 \ln\Big\{f_0(\epsilon)\Big\}\Big], \tag{B.2}$$

$$K = -\frac{1}{h}\frac{1}{T_0}\Big[(E_0)^2(f_0(E_0) - 1) - 2k_{\mathrm{B}}T_0\,(E_0)\ln\Big\{f_0(E_0)\Big\} + 2(k_{\mathrm{B}}T_0)^2\mathrm{Li}_2\Big\{-e^{E_0/(k_{\mathrm{B}}T_0)}\Big\} + \frac{(\pi k_{\mathrm{B}}T_0)^2}{3}\Big]. \tag{B.3}$$

The coefficients, G and L are plotted in Fig. 3.4.

References

[1] S. Datta, "Electronic Transport in Mesoscopic Systems by Supriyo Datta", Cambridge Core (1995) 10.1017/CBO9780511805776 (cit. on p. 1).

[2] C. W. J. Beenakker and H. van Houten, "Quantum Transport in Semiconductor Nanostructures", Solid State Physics **44**, 1–228 (1991) (cit. on p. 1).

[3] J. P. Pekola, O.-P. Saira, V. F. Maisi, A. Kemppinen, M. Möttönen, Y. A. Pashkin, and D. V. Averin, "Single-electron current sources: Toward a refined definition of the ampere", Rev. Mod. Phys. **85**, 1421–1472 (2013) (cit. on p. 2).

[4] G. Fève, A. Mahé, J.-M. Berroir, T. Kontos, B. Plaçais, D. C. Glattli, A. Cavanna, B. Etienne, and Y. Jin, "An On-Demand Coherent Single-Electron Source", Science **316**, 1169–1172 (2007) (cit. on pp. 2, 4, 29, 31, 32, 39, 40).

[5] M. D. Blumenthal, B. Kaestner, L. Li, S. Giblin, T. J. B. M. Janssen, M. Pepper, D. Anderson, G. Jones, and D. A. Ritchie, "Gigahertz quantized charge pumping", Nat. Phys. **3**, 343–347 (2007) (cit. on pp. 2, 3).

[6] R. P. G. McNeil, M. Kataoka, C. J. B. Ford, C. H. W. Barnes, D. Anderson, G. A. C. Jones, I. Farrer, and D. A. Ritchie, "On-demand single-electron transfer between distant quantum dots", Nature **477**, 439–442 (2011) (cit. on pp. 2, 3).

[7] S. Hermelin, S. Takada, M. Yamamoto, S. Tarucha, A. D. Wieck, L. Saminadayar, C. Bauerle, and T. Meunier, "Electrons surfing on a sound wave as a platform for quantum optics with flying electrons", Nature **477**, 435–438 (2011) (cit. on pp. 2, 3).

[8] B. Roche, R.-P. Riwar, B. Voisin, E. Dupont-Ferrier, R. Wacquez, M. Vinet, M. Sanquer, J. Splettstoesser, and X. Jehl, "A two-atom electron pump", Nat. Commun. **4**, 1581 (2013) (cit. on p. 2).

[9] J. Dubois, T. Jullien, F. Portier, P. Roche, A. Cavanna, Y. Jin, W. Wegscheider, P. Roulleau, and D. C. Glattli, "Minimal-excitation states for electron quantum optics using levitons", Nature **502**, 659–663 (2013) (cit. on pp. 2–4, 29, 30, 41).

[10] N. Ubbelohde, F. Hohls, V. Kashcheyevs, T. Wagner, L. Fricke, B. Kästner, K. Pierz, H. W. Schumacher, and R. J. Haug, "Partitioning of on-demand electron pairs", Nat. Nanotechnol. **10**, 46 (2014) (cit. on p. 2).

[11] Y. Sherkunov, N. d'Ambrumenil, P. Samuelsson, and M. Büttiker, "Optimal pumping of orbital entanglement with single-particle emitters", Phys. Rev. B **85**, 081108 (2012) (cit. on p. 2).

[12] E. Bocquillon, V. Freulon, F. D. Parmentier, J.-M. Berroir, B. Plaçais, C. Wahl, J. Rech, T. Jonckheere, T. Martin, C. Grenier, D. Ferraro, P. Degiovanni, and G. Fève, "Electron quantum optics in ballistic chiral conductors", Ann. Phys. **526**, 1–30 (2014) (cit. on p. 2).

[13] Y. Ji, Y. Chung, D. Sprinzak, M. Heiblum, D. Mahalu, and H. Shtrikman, "An electronic Mach–Zehnder interferometer", Nature **422**, 415–418 (2003) (cit. on p. 2).

[14] J. Gabelli, G. Fève, J.-M. Berroir, B. Plaçais, A. Cavanna, B. Etienne, Y. Jin, and D. C. Glattli, "Violation of Kirchhoff's Laws for a Coherent RC Circuit", Science **313**, 499–502 (2006) (cit. on pp. 2, 31, 35).

[15] L. S. Levitov, H. Lee, and G. B. Lesovik, "Electron counting statistics and coherent states of electric current", Journal of Mathematical Physics **37**, 4845 (1998) (cit. on pp. 3, 29, 41).

[16] D. A. Ivanov, H. W. Lee, and L. S. Levitov, "Coherent states of alternating current", Phys. Rev. B **56**, 6839 (1997) (cit. on pp. 3, 29).

[17] J. Keeling, I. Klich, and L. S. Levitov, "Minimal Excitation States of Electrons in One-Dimensional Wires", Phys. Rev. Lett. **97**, 116403 (2006) (cit. on pp. 3, 29).

[18] M. Misiorny, G. Fève, and J. Splettstoesser, "Shaping charge excitations in chiral edge states with a time-dependent gate voltage", Phys. Rev. B **97**, 075426 (2018) (cit. on pp. 3, 29, 35, 36).

[19] C. Bäuerle, D. C. Glattli, T. Meunier, F. Portier, P. Roche, P. Roulleau, S. Takada, and X. Waintal, "Coherent control of single electrons: a review of current progress", Rep. Prog. Phys. **81**, 056503 (2018) (cit. on pp. 3, 29).

[20] J. P. Pekola, J. J. Vartiainen, M. Möttönen, O.-P. Saira, M. Meschke, and D. V. Averin, "Hybrid single-electron transistor as a source of quantized electric current", Nat. Phys. **4**, 120–124 (2008) (cit. on p. 3).

[21] K. Flensberg, A. A. Odintsov, F. Liefrink, and P. Teunissen, "TOWARDS SINGLE-ELECTRON METROLOGY", Int. J. Mod. Phys. B **13**, 2651 (2012) (cit. on p. 3).

[22] C. Leicht, P. Mirovsky, B. Kaestner, F. Hohls, V. Kashcheyevs, E. V. Kurganova, U. Zeitler, T. Weimann, K. Pierz, and H. W. Schumacher, "Generation of energy selective excitations in quantum Hall edge states", Semicond. Sci. Technol. **26**, 055010 (2011) (cit. on p. 3).

[23] M. Vanević, Y. V. Nazarov, and W. Belzig, "Elementary Events of Electron Transfer in a Voltage-Driven Quantum Point Contact", Phys. Rev. Lett. **99**, 076601 (2007) (cit. on p. 4).

[24] M. Vanević, Y. V. Nazarov, and W. Belzig, "Elementary charge-transfer processes in mesoscopic conductors", Phys. Rev. B **78**, 245308 (2008) (cit. on pp. 4, 41).

[25] J. Gabelli and B. Reulet, "Shaping a time-dependent excitation to minimize the shot noise in a tunnel junction", Phys. Rev. B **87**, 075403 (2013) (cit. on pp. 4, 29, 41).

[26] M. Moskalets and M. Büttiker, "Heat production and current noise for single- and double-cavity quantum capacitors", Phys. Rev. B **80**, 081302 (2009) (cit. on pp. 4, 42).

[27] G. Rosselló, F. Battista, M. Moskalets, and J. Splettstoesser, "Interference and multiparticle effects in a Mach-Zehnder interferometer with single-particle sources", Phys. Rev. B **91**, 115438 (2015) (cit. on pp. 4, 32, 41, 42).

[28] F. Ronetti, M. Carrega, D. Ferraro, J. Rech, T. Jonckheere, T. Martin, and M. Sassetti, "Polarized heat current generated by quantum pumping in two-dimensional topological insulators", Phys. Rev. B **95**, 115412 (2017) (cit. on p. 4).

[29] M. F. Ludovico, J. S. Lim, M. Moskalets, L. Arrachea, and D. Sánchez, "Dynamical energy transfer in ac-driven quantum systems", Phys. Rev. B **89**, 161306 (2014) (cit. on p. 4).

[30] F. Zhan, S. Denisov, and P. Hänggi, "Electronic heat transport across a molecular wire: Power spectrum of heat fluctuations", Phys. Rev. B **84**, 195117 (2011) (cit. on p. 4).

[31] A. Crépieux and F. Michelini, "Mixed, charge and heat noises in thermo-electric nanosystems", J. Phys.: Condens. Matter **27**, 015302 (2015) (cit. on p. 4).

[32] P. Eyméoud and A. Crépieux, "Mixed electrical-heat noise spectrum in a quantum dot", Phys. Rev. B **94**, 205416 (2016) (cit. on p. 4).

[33] R. Sánchez and M. Büttiker, "Detection of single-electron heat transfer statistics", EPL **100**, 47008 (2012) (cit. on p. 4).

[34] R. Sánchez and M. Büttiker, "Erratum: Detection of single-electron heat transfer statistics", EPL **104**, 49901 (2013) (cit. on p. 4).

[35] R. Sánchez, B. Sothmann, A. N. Jordan, and M. Büttiker, "Correlations of heat and charge currents in quantum-dot thermoelectric engines", New J. Phys. **15**, 125001 (2013) (cit. on p. 4).

[36] M. Moskalets, "Floquet Scattering Matrix Theory of Heat Fluctuations in Dynamical Quantum Conductors", Phys. Rev. Lett. **112**, 206801 (2014) (cit. on pp. 4, 43).

[37] M. Moskalets, "Erratum: Floquet Scattering Matrix Theory of Heat Fluctuations in Dynamical Quantum Conductors [Phys. Rev. Lett. 112, 206801 (2014)]", Phys. Rev. Lett. **113**, 069902 (2014) (cit. on p. 4).

[38] F. Battista, F. Haupt, and J. Splettstoesser, "Energy and power fluctuations in ac-driven coherent conductors", Phys. Rev. B **90**, 085418 (2014) (cit. on pp. 4, 15, 43).

[39] F. Battista, F. Haupt, and J. Splettstoesser, "Correlations between charge and energy current in ac-driven coherent conductors", J. Phys. Conf. Ser. **568**, 052008 (2014) (cit. on pp. 4, 43).

[40] L. Vannucci, F. Ronetti, J. Rech, D. Ferraro, T. Jonckheere, T. Martin, and M. Sassetti, "Minimal excitation states for heat transport in driven quantum Hall systems", Phys. Rev. B **95**, 245415 (2017) (cit. on pp. 4, 43).

[41] A. Mahé, F. D. Parmentier, E. Bocquillon, J.-M. Berroir, D. C. Glattli, T. Kontos, B. Plaçais, G. Fève, A. Cavanna, and Y. Jin, "Current correlations of an on-demand single-electron emitter", Phys. Rev. B **82**, 201309 (2010) (cit. on p. 4).

[42] F. D. Parmentier, E. Bocquillon, J.-M. Berroir, D. C. Glattli, B. Plaçais, G. Fève, M. Albert, C. Flindt, and M. Büttiker, "Current noise spectrum of a single-particle emitter: Theory and experiment", Phys. Rev. B **85**, 165438 (2012) (cit. on p. 4).

[43] F. Battista, M. Moskalets, M. Albert, and P. Samuelsson, "Quantum Heat Fluctuations of Single-Particle Sources", Phys. Rev. Lett. **110**, 126602 (2013) (cit. on pp. 4, 44).

[44] T. L. van den Berg, F. Brange, and P. Samuelsson, "Energy and temperature fluctuations in the single electron box", New J. Phys. **17**, 075012 (2015) (cit. on pp. 4, 44).

[45] J. S. Lim, R. López, and D. Sánchez, "Dynamic thermoelectric and heat transport in mesoscopic capacitors", Phys. Rev. B **88**, 201304 (2013) (cit. on p. 4).

[46] C. Grenier, R. Hervé, E. Bocquillon, F. D. Parmentier, B. Plaçais, J. M. Berroir, G. Fève, and P. Degiovanni, "Single-electron quantum tomography in quantum Hall edge channels", New J. Phys. **13**, 093007 (2011) (cit. on pp. 4, 50).

[47] P. Samuelsson and M. Büttiker, "Quantum state tomography with quantum shot noise", Phys. Rev. B **73**, 041305 (2006) (cit. on p. 4).

[48] R. Bisognin, A. Marguerite, B. Roussel, M. Kumar, C. Cabart, C. Chapdelaine, A. Mohammad-Djafari, J.-M. Berroir, E. Bocquillon, B. Plaçais, A. Cavanna, U. Gennser, Y. Jin, P. Degiovanni, and G. Fève, "Quantum tomography of electrical currents", Nat. Commun. **10**, 3379–12 (2019) (cit. on pp. 4, 31, 42).

[49] T. Jullien, P. Roulleau, B. Roche, A. Cavanna, Y. Jin, and D. C. Glattli, "Quantum tomography of an electron", Nature **514**, 603 (2014) (cit. on pp. 4, 31, 32, 41, 42).

[50] J. D. Fletcher, P. See, H. Howe, M. Pepper, S. P. Giblin, J. P. Griffiths, G. A. C. Jones, I. Farrer, D. A. Ritchie, T. J. B. M. Janssen, and M. Kataoka, "Clock-Controlled Emission of Single-Electron Wave Packets in a Solid-State Circuit", Phys. Rev. Lett. **111**, 216807 (2013) (cit. on pp. 4, 42, 43).

[51] N. Ubbelohde, F. Hohls, V. Kashcheyevs, T. Wagner, L. Fricke, B. Kästner, K. Pierz, H. W. Schumacher, and R. J. Haug, "Partitioning of on-demand electron pairs", Nat. Nanotechnol. **10**, 46–49 (2015) (cit. on pp. 4, 42).

[52] M. Büttiker, "Quantized transmission of a saddle-point constriction", Phys. Rev. B **41**, 7906–7909 (1990) (cit. on pp. 5, 19, 21).

[53] H. van Houten, L. W. Molenkamp, C. W. J. Beenakker, and C. T. Foxon, "Thermo-electric properties of quantum point contacts", Semicond. Sci. Technol. **7**, B215–B221 (1992) (cit. on pp. 5, 19, 22).

[54] E. N. Bogachek, A. G. Scherbakov, and U. Landman, "Nonlinear peltier effect in quantum point contacts", Solid State Commun. **108**, 851–855 (1998) (cit. on pp. 5, 19).

[55] P. N. Butcher, "Thermal and electrical transport formalism for electronic microstructures with many terminals", J. Phys.: Condens. Matter **2**, 4869–4878 (1990) (cit. on pp. 5, 19, 25).

[56] G. D. Mahan and J. O. Sofo, "The best thermoelectric", Proc. Natl. Acad. Sci. U.S.A. **93**, 7436–7439 (1996) (cit. on pp. 5, 20).

[57] R. S. Whitney, "Most Efficient Quantum Thermoelectric at Finite Power Output", Phys. Rev. Lett. **112**, 130601 (2014) (cit. on pp. 5, 19, 51).

[58] R. S. Whitney, "Finding the quantum thermoelectric with maximal efficiency and minimal entropy production at given power output", Phys. Rev. B **91**, 115425 (2015) (cit. on pp. 5, 19, 51).

[59] R. S. Whitney, "Nonlinear thermoelectricity in point contacts at pinch off: A catastrophe aids cooling", Phys. Rev. B **88**, 064302 (2013) (cit. on p. 5).

[60] J. Meair and P. Jacquod, "Scattering theory of nonlinear thermoelectricity in quantum coherent conductors", J. Phys.: Condens. Matter **25**, 082201 (2013) (cit. on pp. 5, 23, 24).

[61] F. L. Curzon and B. Ahlborn, "Efficiency of a Carnot engine at maximum power output", Am. J. Phys **43**, 22 (1975) (cit. on pp. 5, 20).

[62] C. Van den Broeck, "Thermodynamic Efficiency at Maximum Power", Phys. Rev. Lett. **95**, 190602 (2005) (cit. on pp. 5, 20).

[63] M. Esposito, R. Kawai, K. Lindenberg, and C. Van den Broeck, "Efficiency at Maximum Power of Low-Dissipation Carnot Engines", Phys. Rev. Lett. **105**, 150603 (2010) (cit. on pp. 5, 20).

[64] B. K. Agarwalla and D. Segal, "Assessing the validity of the thermodynamic uncertainty relation in quantum systems", Phys. Rev. B **98**, 155438 (2018) (cit. on pp. 5, 20).

[65] K. Macieszczak, K. Brandner, and J. P. Garrahan, "Unified Thermodynamic Uncertainty Relations in Linear Response", Phys. Rev. Lett. **121**, 130601 (2018) (cit. on pp. 5, 20).

[66] Y. Hasegawa and T. Van Vu, "Generalized thermodynamic uncertainty relation via fluctuation theorem", arXiv (2019), eprint: 1902.06376 (cit. on p. 5).

[67] D. A. Ryndyk, "Landauer-Büttiker Method", SpringerLink, 17–54 (2016) (cit. on p. 7).

[68] Y. M Blanter and M Büttiker, "Shot noise in mesoscopic conductors", Physics reports **336**, 1–166 (2000) (cit. on p. 7).

[69] W. Li and L. E. Reichl, "Floquet scattering through a time-periodic potential", Phys. Rev. B **60**, 15732–15741 (1999) (cit. on p. 7).

[70] M. Moskalets and M. Büttiker, "Floquet scattering theory of quantum pumps", Phys. Rev. B **66**, 205320 (2002) (cit. on pp. 7, 12, 14).

[71] N. Dashti, "Charge and energy noise from on-demand electron sources", PhD thesis (2017) (cit. on pp. 8, 12, 55).

[72] M Büttiker, "Scattering theory of current and intensity noise correlations in conductors and wave guides", Phys. Rev. B **46**, 12485 (1992) (cit. on p. 10).

[73] M. Büttiker, *Scattering theory of current and intensity noise correlations in conductors and wave guides*, 1992 (cit. on p. 11).

[74] Ya. M. Blanter and M. Büttiker, "Shot noise in mesoscopic conductors", Phys. Rep. **336**, 1–166 (2000) (cit. on pp. 11, 41).

[75] M. Moskalets and M. Büttiker, "Adiabatic quantum pump in the presence of external ac voltages", Phys. Rev. B **69**, 205316 (2004) (cit. on p. 12).

[76] M. Grifoni and P. Hänggi, "Driven quantum tunneling", Phys. Rep. **304**, 229–354 (1998) (cit. on p. 12).

[77] M. V Moskalets, *Scattering matrix approach to non-stationary quantum transport* (World Scientific, 2011) (cit. on pp. 12, 55).

[78] B. J. van Wees, H. van Houten, C. W. J. Beenakker, J. G. Williamson, L. P. Kouwenhoven, D. van der Marel, and C. T. Foxon, "Quantized conductance of point contacts in a two-dimensional electron gas", Phys. Rev. Lett. **60**, 848–850 (1988) (cit. on p. 19).

[79] G. Bevilacqua, G. Grosso, G. Menichetti, and G. Pastori Parravicini, "Thermoelectric efficiency of nanoscale devices in the linear regime", Phys. Rev. B **94**, 245419 (2016) (cit. on pp. 19, 20).

[80] S. Pilgram, D. Sánchez, and R. López, "Quantum point contacts as heat engines", Physica E **82**, 310–313 (2016) (cit. on pp. 19, 20, 25).

[81] N. Nakpathomkun, H. Q. Xu, and H. Linke, "Thermoelectric efficiency at maximum power in low-dimensional systems", Phys. Rev. B **82**, 235428 (2010) (cit. on pp. 20–22, 25).

[82] G. Bevilacqua, G. Grosso, G. Menichetti, and G. Pastori Parravicini, "Thermoelectric regimes of materials with peaked transmission function", arXiv (2018), eprint: 1809.05449 (cit. on pp. 20, 25).

[83] X. Luo, C. Li, N. Liu, R. Li, J. He, and T. Qiu, "The impact of energy spectrum width in the energy selective electron low-temperature thermionic heat engine at maximum power", Phys. Lett. A **377**, 1566–1570 (2013) (cit. on pp. 20, 25).

[84] M. Esposito, K. Lindenberg, and C. Van den Broeck, "Thermoelectric efficiency at maximum power in a quantum dot", EPL **85**, 60010 (2009) (cit. on pp. 20, 25).

[85] M. A. Çipiloğlu, S. Turgut, and M. Tomak, "Nonlinear Seebeck and Peltier effects in quantum point contacts", Phys. Status solidi B **241**, 2575–2585 (2004) (cit. on pp. 20, 25).

[86] R. Taboryski, A. Kristensen, C. B. So/rensen, and P. E. Lindelof, "Conductance-quantization broadening mechanisms in quantum point contacts", Phys. Rev. B **51**, 2282–2286 (1995) (cit. on pp. 21, 22).

[87] A. S. Dzurak, C. G. Smith, L. Martin-Moreno, M. Pepper, D. A. Ritchie, G. A. C. Jones, and D. G. Hasko, "Thermopower of a one-dimensional ballistic constriction in the non-linear regime", J. Phys.: Condens. Matter **5**, 8055–8064 (1993) (cit. on pp. 21, 22).

[88] Fertig and Halperin, "Transmission coefficient of an electron through a saddle-point potential in a magnetic field", Phys. Rev. B **36**, 7969–7976 (1987) (cit. on p. 21).

[89] W. H. Miller, "Semiclassical Treatment of Multiple Turning-Point Problems—Phase Shifts and Eigenvalues", J. Chem. Phys. **48**, 1651–1658 (1968) (cit. on p. 22).

[90] T. Christen and M. Büttiker, "Gauge-invariant nonlinear electric transport in mesoscopic conductors", EPL **35**, 523–528 (1996) (cit. on pp. 23, 24, 26).

[91] M. Büttiker and T. Christen, "Admittance and Nonlinear Transport in Quantum Wires, Point Contacts, and Resonant Tunneling Barriers", SpringerLink, 259–289 (1997) (cit. on pp. 23, 24, 26).

[92] D. Sánchez and R. López, "Scattering Theory of Nonlinear Thermoelectric Transport", Phys. Rev. Lett. **110**, 026804 (2013) (cit. on pp. 23, 26).

[93] M. H. Pedersen, S. A. van Langen, and M. Büttiker, "Charge fluctuations in quantum point contacts and chaotic cavities in the presence of transport", Phys. Rev. B **57**, 1838–1846 (1998) (cit. on p. 23).

[94] M. Büttiker and D. Sánchez, "Interaction-induced magnetic field asymmetry of nonlinear mesoscopic electrical transport", Int. J. Quantum Chem. **105**, 906–913 (2005) (cit. on p. 24).

[95] G. Benenti, G. Casati, K. Saito, and R. S. Whitney, "Fundamental aspects of steady-state conversion of heat to work at the nanoscale", Phys. Rep. **694**, 1–124 (2017) (cit. on pp. 24, 25).

[96] M. Moskalets and G. Haack, "Single-electron coherence: Finite temperature versus pure dephasing", Physica E **75**, 358–369 (2016) (cit. on pp. 31, 50).

[97] D. Ferraro, A. Feller, A. Ghibaudo, E. Thibierge, E. Bocquillon, G. Fève, Ch. Grenier, and P. Degiovanni, "Wigner function approach to single electron coherence in quantum Hall edge channels", Phys. Rev. B **88**, 205303 (2013) (cit. on pp. 31, 50).

[98] G. Haack, M. Moskalets, J. Splettstoesser, and M. Büttiker, "Coherence of single-electron sources from Mach-Zehnder interferometry", Phys. Rev. B **84**, 081303 (2011) (cit. on pp. 32, 41).

[99] P. P. Hofer and C. Flindt, "Mach-Zehnder interferometry with periodic voltage pulses", Phys. Rev. B **90**, 235416 (2014) (cit. on pp. 32, 41).

[100] S. Juergens, J. Splettstoesser, and M. Moskalets, "Single-particle interference versus two-particle collisions", EPL **96**, 37011 (2011) (cit. on pp. 32, 41).

[101] C. Grenier, R. Hervé, E. Bocquillon, F. D. Parmentier, B. Plaçais, J. M. Berroir, G. Fève, and P. Degiovanni, "Single-electron quantum tomography in quantum Hall edge channels", New J. Phys. **13**, 093007 (2011) (cit. on pp. 32, 41, 42).

[102] E. Bocquillon, F. D. Parmentier, C. Grenier, J.-M. Berroir, P. Degiovanni, D. C. Glattli, B. Plaçais, A. Cavanna, Y. Jin, and G. Fève, "Electron Quantum Optics: Partitioning Electrons One by One", Phys. Rev. Lett. **108**, 196803 (2012) (cit. on pp. 32, 41, 42).

[103] E. Bocquillon, V. Freulon, J.-M. Berroir, P. Degiovanni, B. Plaçais, A. Cavanna, Y. Jin, and G. Fève, "Separation of neutral and charge modes in one-dimensional chiral edge channels", Nat. Commun. **4**, 1839 (2013) (cit. on pp. 32, 41).

[104] É. Thibierge, D. Ferraro, B. Roussel, C. Cabart, A. Marguerite, G. Fève, and P. Degiovanni, "Two-electron coherence and its measurement in electron quantum optics", Phys. Rev. B **93**, 081302 (2016) (cit. on pp. 32, 41).

[105] T. Jonckheere, J. Rech, C. Wahl, and T. Martin, "Electron and hole Hong-Ou-Mandel interferometry", Phys. Rev. B **86**, 125425 (2012) (cit. on pp. 32, 41).

[106] E. Bocquillon, V. Freulon, J.-M. Berroir, P. Degiovanni, B. Plaçais, A. Cavanna, Y. Jin, and G. Fève, "Coherence and Indistinguishability of Single Electrons Emitted by Independent Sources", Science **339**, 1054–1057 (2013) (cit. on pp. 32, 41).

[107] M. Moskalets and M. Büttiker, "Spectroscopy of electron flows with single- and two-particle emitters", Phys. Rev. B **83**, 035316 (2011) (cit. on pp. 32, 41).

[108] S. Ol'khovskaya, J. Splettstoesser, M. Moskalets, and M. Büttiker, "Shot Noise of a Mesoscopic Two-Particle Collider", Phys. Rev. Lett. **101**, 166802 (2008) (cit. on pp. 32, 41).

[109] C. Wahl, J. Rech, T. Jonckheere, and T. Martin, "Interactions and Charge Fractionalization in an Electronic Hong-Ou-Mandel Interferometer", Phys. Rev. Lett. **112**, 046802 (2014) (cit. on pp. 32, 41).

[110] V. Freulon, A. Marguerite, J.-M. Berroir, B. Plaçais, A. Cavanna, Y. Jin, and G. Fève, "Hong-Ou-Mandel experiment for temporal investigation of single-electron fractionalization", Nat. Commun. **6**, 6854 (2015) (cit. on pp. 32, 41).

[111] D. Litinski, P. W. Brouwer, and M. Filippone, "Interacting mesoscopic capacitor out of equilibrium", Phys. Rev. B **96**, 085429 (2017) (cit. on p. 35).

[112] F. D. Parmentier, A. Mahé, A. Denis, J.-M. Berroir, D. C. Glattli, B. Plaçais, and G. Fève, "A high sensitivity ultralow temperature RF conductance and noise measurement setup", Rev. Sci. Instrum. **82**, 013904 (2011) (cit. on p. 41).

[113] D. C. Glattli, "Quantum shot noise of conductors and general noise measurement methods", Eur. Phys. J. Spec. Top. **172**, 163–179 (2009) (cit. on p. 41).

[114] P. Samuelsson and M. Büttiker, "Quantum state tomography with quantum shot noise", Phys. Rev. B **73**, 041305 (2006) (cit. on p. 42).

[115] J. Waldie, P. See, V. Kashcheyevs, J. P. Griffiths, I. Farrer, G. A. C. Jones, D. A. Ritchie, T. J. B. M. Janssen, and M. Kataoka, "Measurement and control of electron wave packets from a single-electron source", Phys. Rev. B **92**, 125305 (2015) (cit. on p. 42).

[116] M. Moskalets and G. Haack, "Heat and charge transport measurements to access single-electron quantum characteristics", Phys. Status solidi B **254**, 1600616 (2017) (cit. on p. 43).

[117] F. Ronetti, L. Vannucci, D. Ferraro, T. Jonckheere, J. Rech, T. Martin, and M. Sassetti, "Hong-Ou-Mandel heat noise in the quantum Hall regime", Phys. Rev. B **99**, 205406 (2019) (cit. on p. 43).

[118] Y. Utsumi, O. Entin-Wohlman, A. Aharony, T. Kubo, and Y. Tokura, "Fluctuation theorem for heat transport probed by a thermal probe electrode", Phys. Rev. B **89**, 205314 (2014) (cit. on p. 44).

[119] S. Gasparinetti, K. L. Viisanen, O.-P. Saira, T. Faivre, M. Arzeo, M. Meschke, and J. P. Pekola, "Fast Electron Thermometry for Ultrasensitive Calorimetric Detection", Phys. Rev. Appl. **3**, 014007 (2015) (cit. on p. 44).

[120] S. Jezouin, F. D. Parmentier, A. Anthore, U. Gennser, A. Cavanna, Y. Jin, and F. Pierre, "Quantum Limit of Heat Flow Across a Single Electronic Channel", Science **342**, 601–604 (2013) (cit. on p. 44).

[121] K. Schwab, E. A. Henriksen, J. M. Worlock, and M. L. Roukes, "Measurement of the quantum of thermal conductance", Nature **404**, 974–977 (2000) (cit. on p. 44).

[122] D. Gresta, M. Real, and L. Arrachea, "Optimal thermoelectricity with quantum spin-Hall edge states", arXiv (2019), eprint: 1904.12688 (cit. on p. 51).

[123] M. Moskalets, P. Samuelsson, and M. Büttiker, "Quantized Dynamics of a Coherent Capacitor", Phys. Rev. Lett. **100**, 086601 (2008) (cit. on p. 55).